

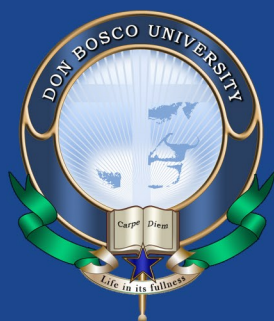


ISSN: 2582-0257

# ADBU Journal of Electrical and Electronics Engineering

An International Peer Reviewed Open Access Journal exploring innovative research findings in Electrical and Electronics Engineering & Technology and its Allied sciences

Volume 1 Issue 2



**ASSAM  
DON BOSCO  
UNIVERSITY**



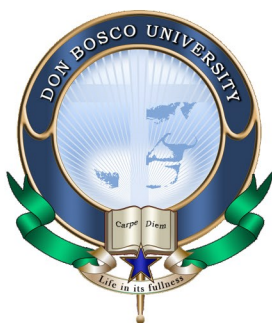


ISSN: 2582-0257

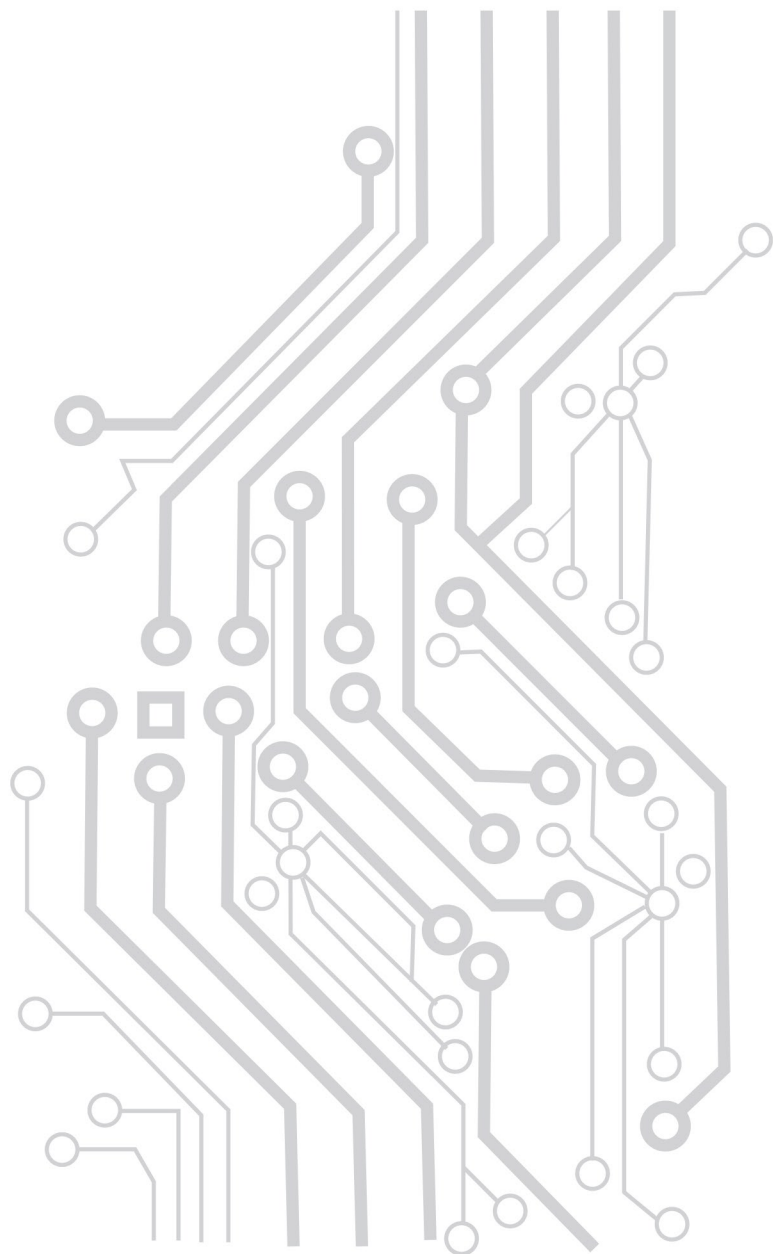
# ADBU Journal of Electrical and Electronics Engineering

An International Peer Reviewed Open Access Journal exploring innovative research findings in Electrical and Electronics Engineering & Technology and its Allied sciences

**Volume 1    Issue 2**



**ASSAM  
DON BOSCO  
UNIVERSITY**



# ADBU Journal of Electrical and Electronics Engineering (AJEEE)

ISSN: 2582-0257

© All rights reserved by the Department of Electrical and Electronics Engineering (EEE), Assam Don Bosco University, Airport Road, Azara, Guwahati, India- 781017.

Website: [www.tinyurl.com/ajeee-adbu](http://www.tinyurl.com/ajeee-adbu) , <http://journals.dbuniversity.ac.in/ojs/index.php/AJEEE>

## Volume 1, Issue 2

Published in September, 2017

### Editor-in-Chief :

Dr. Shakuntala Laskar, Professor & HOD, Dept. of EEE, Assam Don Bosco University

### Editor :

Mr. Bikramjit Goswami, Assistant Professor, Dept. of EEE, Assam Don Bosco University

### International Advisory Board :

- Dr. Sridhar Chouhan, P.E., Leidos Engineering, LLC, Hendersonville, TN, USA.
- Prof. Dr. Esteban Tlelo-Cuautle, Department of Electronics, National Institute of Astrophysics, Optics and Electronics, Mexico.
- Prof. Dr. Akhtar Kalam, Head of External Engagement, Leader – Smart Energy Research Unit, College of Engineering and Science, Victoria University, Australia.
- Prof. Ir. Dr. Hazlie Bin Mokhlis, Department of Electrical Engineering, Deputy Dean (Undergraduate Studies), Faculty of Engineering, University of Malaya, Malaysia.
- Prof. Dr. Sisil Kumarawadu, SMIEEE, Dept. of Electrical Engineering, Faculty of Engineering, University of Moratuwa, Sri Lanka.
- Prof. Dr. Durlav Hazarika, Dept. of Electrical Engineering, Assam Engineering College, India.
- Mr. Shauquat Alam, Sr. Vice President (Investment & Strategy Solutions), Sovereign Infrastructure Development Company Limited, UK.
- Dr. Sadhan Mahapatra, Department of Energy, Tezpur University, India.
- Dr. Bani Kanta Talukdar, Dept. of Electrical Engineering, Assam Engineering College, India.

### Associate Editors :

- Mr. Jesif Ahmed, Assam Don Bosco University.
- Ms. Pushpanjalee Konwar, Assam Don Bosco University.
- Mr. Jyoti Kumar Barman, Assam Don Bosco University.
- Ms. Smriti Dey, Assam Don Bosco University.
- Mr. Gitu Das, Assam Don Bosco University.
- Mr. Papul Changmai, Assam Don Bosco University.
- Mr. Hironmay Deb, Assam Don Bosco University.
- Mr. Sunil Deka, Assam Don Bosco University.

### Cover Design:

Jiwan Ekka & Jesif Ahmed



This Journal is published by the Department of EEE, Assam Don Bosco University, Azara, Assam (India) under the [Creative Commons Attribution 4.0 International License \(CC-BY\)](https://creativecommons.org/licenses/by/4.0/).

# Contents

---

Sl. No.	Articles and Authors	Pg. No.
1.	Performance Analysis of Non-linear Jacketed CSTR Based on Different Control Strategies - <i>Pranjal Kalita and Jyoti Kumar Barman</i>	1
2.	Optimization of DC Microgrid for Renewable Energy Integration - <i>Risalin Lyngdoh Mairang</i>	8
3.	Electrical Methods of Soil Moisture Measurement: A Review - <i>Muktimani Brahma and Bikramjit Goswami</i>	14
4.	A Review on Light Trapping Capacities of Different Photovoltaic Cells - <i>Nayanjyoti Deka and Papul Changmai</i>	18
5.	A Review on Wireless Power Transfer - <i>Parveen Kaur</i>	29
6.	Distributed Optical Fiber Sensor and its Various Applications - <i>Madhushree Sharma and Shakuntala Laskar</i>	33



# Performance Analysis of Non-linear Jacketed CSTR based on Different Control Strategies

Pranjal Kalita<sup>1</sup>, Jyoti Kumar Barman<sup>2</sup>

<sup>1,2</sup> Department of Electrical and Electronics Engineering, School of Technology, Assam Don Bosco University, Airport Road, Azara, Guwahati -781017, Assam, INDIA.

<sup>1</sup>pranjaladbu@gmail.com, <sup>2</sup>jyoti.barman@dbuniversity.ac.in\*

**Abstract:** This paper aims at finding the optimum controller for a jacketed Continuous Stirred Tank Reactor (CSTR) under non-ideal conditions. Various conventional control methods show poor response for non-linear processes. This paper outlines the design procedure of the Internal Model Controller (IMC) and Model Reference Adaptive Control (MRAC). The performance of the jacketed CSTR process is analyzed based on Internal Model Control and adaptive control. Simulation results have been compared with conventional PID control.

**Keywords:** Continuous Stirred Tank Reactor (CSTR), Model Reference Adaptive Control (MRAC), Internal Model Controller (IMC), Dead space, PID Controller

## 1. Introduction

Designing a controller assuming linear behaviour for the continuous stirred tank reactor (CSTR) will lead to poor performances. In the case of ideal behaviour the dead space and bypass is not considered, which affects the transient of the system and the desired output concentration.

In this paper, the following works have been done:

- Modelling of a non-linear CSTR with dead space and bypass has been shown in Section 2.
- Stability analysis of the practical system (as per modelling done in Section 2) has been shown in Section 3.
- Application of different control techniques and comparison of all the techniques for the controlled CSTR has been investigated in Section 3.

## 2. Mathematical Modelling of Non-Linear Jacketed CSTR

Figure 1 shows the basic schematic diagram of a jacketed CSTR, in which a simple irreversible, exothermic reaction  $A \rightarrow B$  is taking place. The reactor is surrounded by a jacket where mixing is taking place at low temperature than the reactor. Energy is passed through the reactor wall into the jacket, removing the heat generated by the reaction [1,2].

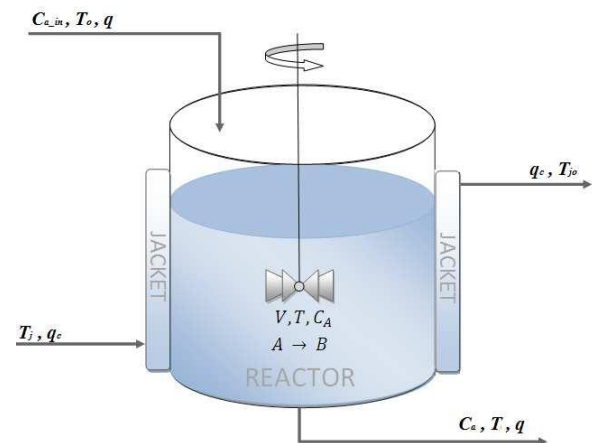


**Figure 1:** Schematic diagram of a continuous stirred tank reactor [2]

The feed material composition  $C_{a,in}$  enters the reactor at temperature  $T_o$  at a volumetric flow rate of  $q$ . The product is withdrawn from the reactor at same volumetric flow rate  $q$ .

In a jacketed CSTR, the heat is added or removed by virtue of the temperature difference between a jacket fluid and the reactor fluid. As the reaction undergoing within the reactor is considered exothermic, heat will be evolved for the reactor and hence a coolant will flow through the jacket at a flow rate of  $q_c$  fed at a temperature of  $T_j$ .

The non-uniform mixing in non-linear CSTR results in bypassing and dead space. When perfect mixing does not takes place in the overall volume and results in less reactor volume than in case of ideal behaviour, due to which it results in rapid decay of transient than in case of ideal case. In case of bypass, the volumetric flow rate will be

less than that of the volumetric flow in the ideal behaviour case, which results in a slower decay of the transient as compared to the ideal case. The schematic representation of the non-linear CSTR combined with dead space and bypass is shown in Figure 2.

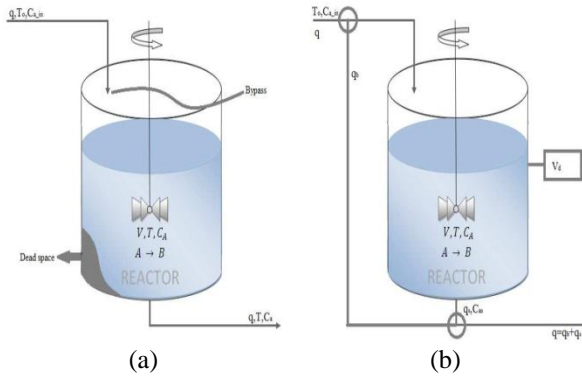


**Figure 2:** Non-linear CSTR: (a) Real system; (b) Model system [2]

**2.1 Material balance of Component A**

Considering an irreversible, exothermic first-order chemical reaction  $A \rightarrow B$ , taking place in non-linear condition.

$$\frac{dC_a}{dt} = \frac{q}{\alpha V} (C_{a\_in} - C_a) - k_o \exp\left(\frac{-E_a}{R(T - \beta T_o)}\right) \left(\frac{C_a - \beta C_{a\_in}}{1 - \beta}\right) \dots\dots (1)$$

Where  $C_{a\_in}$  is the feed material concentration,  $C_a$  is the concentration of component A,  $k_o$  is the frequency factor,  $E_a$  is the activation energy,  $R$  is the gas constant,  $T$  is the temperature,  $\alpha$  is the dead space and  $\beta$  is the bypass.

**2.2 Reactor Energy Balance**

According to the principle of conservation of energy:

(Rate of energy accumulation) = (Rate of energy input) - (Rate of energy output) - (Rate of energy removed by the coolant) + (Rate of energy added by exothermic reaction)

$$\frac{dT}{dt} = \frac{q}{V} (T_o - T) - \alpha \left(\frac{-\Delta H}{\rho C_p}\right) k_o \exp\left(\frac{-E_a}{R(T - \beta T_o)}\right) \left(\frac{C_a - \beta C_{a\_in}}{1 - \beta}\right) + \left(\frac{\rho_c C_{pc}}{\rho C_p V}\right) q_c \left[1 - \exp\left(\frac{-hA}{q_c \rho_c C_{pc}}\right)\right] (T_j - T) \dots\dots\dots (2)$$

Where  $-\Delta H$  is the heat of the reaction,  $UA$  is the heat transfer coefficient,  $T_o$  is the feed temperature,  $T_j$  is the jacketed temperature,  $C_p$  is the heat capacity,  $\rho$  is the density.

**2.3 State variable form of the equation**

Equations (1) and (2) are expressed in the standard state variable form as follows:

$$\frac{dC_a}{dt} = f_1(C_a, T) = \frac{q}{\alpha V} (C_{a\_in} - C_a) - k_o \exp\left(\frac{-E_a}{R(T - \beta T_o)}\right) \left(\frac{C_a - \beta C_{a\_in}}{1 - \beta}\right) \dots\dots\dots (3)$$

$$\frac{dT}{dt} = f_2(C_a, T) = \frac{q}{V} (T_o - T) - \alpha \left(\frac{-\Delta H}{\rho C_p}\right) k_o \exp\left(\frac{-E_a}{R(T - \beta T_o)}\right) \left(\frac{C_a - \beta C_{a\_in}}{1 - \beta}\right) + \left(\frac{\rho_c C_{pc}}{\rho C_p V}\right) q_c \left[1 - \exp\left(\frac{-hA}{q_c \rho_c C_{pc}}\right)\right] (T_j - T) \dots\dots\dots (4)$$

**2.4 Linearization**

The linearization method is applied to non-linear CSTR model to obtain the state space representation. The state, input and the output vector is defined by the following:

$$x = \begin{bmatrix} C_a - C_{as} \\ T - T_s \end{bmatrix}, u = \begin{bmatrix} 0 \\ T_j - T_{js} \end{bmatrix}, y = \begin{bmatrix} C_a - C_{as} \\ T - T_s \end{bmatrix}$$

Where  $C_{as}$  is the steady-state value of effluent concentration,  $T_s$  is the steady-state value of reactor temperature,  $q_s$  is the steady-state value of feed flow rate,  $q_{cs}$  is the steady-state value of the coolant flow rate.

The state space matrices for the CSTR model are derived from the corresponding Jacobian matrix:

$$A = \begin{bmatrix} A_{11} & A_{12} \\ A_{21} & A_{22} \end{bmatrix} = \begin{bmatrix} \frac{\delta f_1}{\delta x_1} & \frac{\delta f_1}{\delta x_2} \\ \frac{\delta f_2}{\delta x_1} & \frac{\delta f_2}{\delta x_2} \end{bmatrix}$$

$$A_{11} = \frac{df_1}{dx_1} = \frac{q}{\alpha V} - \frac{k_o}{1 - \beta} \exp\left(\frac{-E_a(1 - \beta)}{R(T - \beta T_o)}\right)$$

$$A_{12} = \frac{df_1}{dx_2} = \frac{E_a k_o (C_a - \beta C_{a\_in})}{R(T - \beta T_o)^2} \exp\left(\frac{-E_a(1 - \beta)}{R(T - \beta T_o)}\right)$$

$$A_{21} = \frac{df_2}{dx_1} = \alpha \left(\frac{\Delta H}{\rho C_p}\right) k_o \exp\left(\frac{-E_a(1 - \beta)}{R(T - \beta T_o)}\right) \left(\frac{1}{1 - \beta}\right)$$

$$A_{22} = \frac{df_2}{dx_2} = -\frac{q}{V} - \frac{\alpha \Delta H k_o E_a (C_a - \beta C_{a\_in})}{\rho C_p R(T - \beta T_o)^2} \exp\left(\frac{-E_a(1 - \beta)}{R(T - \beta T_o)}\right) -$$

$$\left(\frac{\rho_c C_{pc}}{\rho C_p V}\right) \left[1 - \exp\left(\frac{-hA}{q_c \rho_c C_{pc}}\right)\right]$$

$$B = \begin{bmatrix} B_{11} \\ B_{21} \end{bmatrix} = \begin{bmatrix} \frac{\delta f_1}{\delta u_1} \\ \frac{\delta f_2}{\delta u_1} \end{bmatrix}$$

$$B_{11} = \frac{\delta f_1}{\delta u_1} = 0$$

$$B_{21} = \frac{\delta f_2}{\delta u_1} = \frac{\rho_c C_{pc}}{\rho C_p V} \left[ 1 - \exp\left(\frac{-hA}{q_c \rho_c C_{pc}}\right) \right]$$

**Table 1:** Steady state operating data

Symb ol	Parameters	Values
$C_a$	Reactor Concentration	0.0882 mol / l
$T$	Reactor temperature	441.2K
$q_c$	Coolant flow rate	100l / min
$q$	Feed flow rate	100l / min
$C_{a\_in}$	Feed concentration	1mol / l
$T_o$	Inlet temperature	350K
$T_j$	Inlet jacket temperature	350K
$V$	CSTR volume	100l
$hA$	Heat transfer coefficient	$7 \times 10^5 \text{ cal / (min K)}$
$k_o$	Reaction rate constant	$7.2 \times 10^{10} \text{ min}^{-1}$
$\frac{E_a}{R}$	Activation energy term	$1 \times 10^4 \text{ K}$
$-\Delta H$	Heat of reaction	$-2 \times 10^5 \text{ cal / mol}$
$\rho, \rho_c$	Liquid densities	$1 \times 10^3 \text{ g / l}$
$C_p, C_{pc}$	Specific heat	$1 \text{ cal / (g / K)}$

The operating points for the local linear models of the non-linear CSTR for both the cases are presented in Table 2.

**Table 2:** The operating points for the local linear models of the non-linear CSTR

Feed flow (l/min)	Coolant flow (l/min)	Effluent Conc. (mol/l)	Reactor Temp. (K)
103	97	0.2442	427.9

The matrices A and B can be determined using the values mentioned in the above table and the transfer function that relate the input and output.

$$A = \begin{bmatrix} -16.64 & 0.486 \\ 3528 & -11.75 \end{bmatrix}, B = \begin{bmatrix} 0 \\ 0.99908 \end{bmatrix}, C = [0,1], D = 0$$

The continuous time transfer function is given as:

$$g_p(s) = \frac{0.991s + 16.62}{s^2 + 28.39s + 24.06}$$

### 2.5 Stability Analysis of Non-Linear CSTR

Stability analysis of nonlinear continuous CSTR system is done by using Lyapunov stability.

Given a nonlinear differential equation,

$$\dot{x} = f(x, t)$$

And a scalar function  $V(x)$ ,

If

1.  $V(x)$  is positive definite, and
2.  $\dot{V}(x)$ , the derivative of  $V(x)$ , is negative definite, and
3.  $V(x) \rightarrow \infty$ , as  $\|x\| \rightarrow \infty$

Then, the system  $\dot{x} = f(x, t)$  is globally asymptotically stable.

To derive the necessary condition for stability  $\dot{x} = Ax$  using the method of Lyapunov, the above-mentioned steps should be followed where the possible Lyapunov function in quadratic form is chosen as:  $V(x) = x^T P x$

The Lyapunov function will be positive definite if the matrix  $P$  is symmetric positive definite. The time derivative is given by:

$$\dot{V}(x) = x^T (A^T P + AP) x$$

Where the convenience matrix  $Q = -(A^T P + AP)$

So, if ‘ $-Q$ ’ is negative definite, (or alternatively  $Q$  is positive definite,  $Q > 0$ ), then the system is stable [4,5].

In the case of non-linear CSTR the value of ‘ $P$ ’ is:

$$P = \begin{bmatrix} 144.28 & -0.6807 \\ -0.6807 & 0.0144 \end{bmatrix}$$

Positive definiteness can be found using MATLAB software by a doing Cholesky decomposition using the function  $[R,p] = \text{chol}(A)$ . In this given case, ‘ $P$ ’ is 1. Hence,  $P$  is positive definite and therefore the system is stable.

## 3. Control Strategies for Non-Ideal CSTR

### 3.1 Adaption Law

The adaption law attempts to find a set of parameters that minimizes the error between the plant and the model outputs. To do this, the parameters of the controller are incrementally adjusted until the error has reduced to zero [12]. A number of adaption laws have been developed to

date. The two main types are the gradient and the Lyapunov approach [12], and we have used the gradient approach [7].

### 3.1.1 Model Reference Adaptive Control

Model Reference Adaptive Control (MRAC) is considered to be an important adaptive controller. In the case of MRAC, the desired performance is expressed in terms of a reference model that provides a desired response to the command signal.

The standard implementation of MRAC is shown in Figure 3. It is composed of two loops. The first loop is the ordinary feedback loop that consists of the process and the controller, which is known as the inner loop. The second loop, also known as the outer loop comprises of the adjusting mechanism. The difference between the plant output and the reference model output provides the error signal and parameter change will be based upon that error signal [8,9].

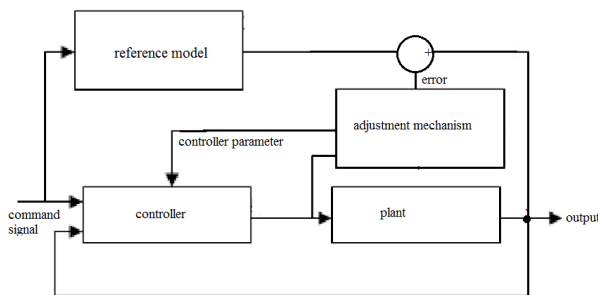


Figure 3: Model Reference Adaptive Controller

The adjusting mechanism will be based upon two methods, the gradient method and the Lyapunov method [10].

### 3.1.2 Adaptive Control Design

For implementing the basic adaptive controller using MATLAB Simulink, the plant transfer function is to be defined which is to be controlled. The continuous time transfer function of the system is given as:

$$g_p(s) = \frac{1.458s + 11.65}{s^2 + 3.434s + 3.342}$$

Secondly, a model should be defined that will match with the given plant. To determine the model, the characteristics should be defined. In order to define the characteristics, an arbitrary second-order model will be selected [12] as:

$$g_m(s) = \frac{\omega_n^2}{s^2 + 2\xi\omega_n s + \omega_n^2}$$

The damping factor  $\xi$  and the natural frequency  $\omega_n$  should be determined in order to get the required performance.

For the concentration control, a maximum overshoot of 5% and the settling time less than 3 is selected [8]. The following mentioned condition is used to determine the damping factor  $\xi$  and the natural frequency  $\omega_n$  [12].

$$\xi = \frac{\ln M_p / 100}{-\pi} \sqrt{\frac{1}{1 + \left(\frac{\ln M_p / 100}{-\pi}\right)^2}}$$

$$\omega_n = \frac{3}{\xi T_s}$$

Based on the above formula, the damping factor and the natural frequency are determined as:  $\xi = 0.713, \omega_n = 2.134$

Therefore, the transfer function for the model is defined as

$$g_m(s) = \frac{4.76}{s^2 + 3.1s + 4.76}$$

### 3.1.3 MIT Rule

To present the MIT rule, we can consider a closed loop system in which the controller has one adjustable parameter. The desired closed loop response is specified by a model output  $Y_m$ . The error ( $e$ ) is the difference between the output of the system ( $Y$ ) and the output of the reference model ( $Y_m$ ) [11,12,14].

The Modeling error  $e$  is given by equation [12] :

$$e = Y - Y_m$$

One possibility is to adjust parameters in such a way that the loss function  $J(\theta)$  is minimized.

$$J(\theta) = \frac{1}{2}e^2$$

To make  $J$  small, it is reasonable to change the parameters in the direction of the negative gradient of  $J$  [14].

$$\frac{d\theta}{dt} = -\gamma \frac{\delta J}{\delta \theta} = -\gamma e \frac{\delta e}{\delta \theta}$$

This is the celebrated MIT rule. The partial derivative  $\frac{\delta e}{\delta \theta}$  is called the sensitivity derivative of the system, tells how the error is influenced by the adjustable parameter. Here,  $\gamma$  is called adaptation gain.

### 3.2 Internal Model Control System configuration

The IMC configuration is designed for setting up a comparison between the process and model output

to form a standard feedback structure. Figure 4 shows the basic IMC implementation in the process transfer function [6].

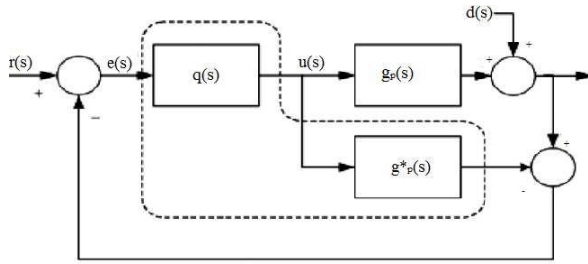


**Figure 4:** IMC configuration

Considering the IMC based PID design procedure for a second order system of CSTR process model of type:

$$\tilde{g}_p(s) = \frac{(\beta s + 1)}{(\tau^2 s^2 + 2\xi\tau s + 1)}$$

$$\tilde{g}_p(s) = \tilde{g}_{p+}(s) \tilde{g}_{p-}(s) = \frac{(\beta s + 1)}{(\tau^2 s^2 + 2\xi\tau s + 1)}$$

$$\tilde{q}(s) = \tilde{g}_{p-}^{-1}(s) = \frac{\tau^2 s^2 + 2\xi\tau s + 1}{(\beta s + 1)}$$

$$q(s) = \tilde{q}(s) f(s) = \tilde{g}_{p-}^{-1}(s) f(s) = \frac{\tau^2 s^2 + 2\xi\tau s + 1}{(\beta s + 1)} \frac{1}{\lambda s + 1}$$

$$g_c(s) = \frac{q(s)}{1 - \tilde{q}(s) \tilde{g}(s)} = \frac{\frac{\tau^2 s^2 + 2\xi\tau s + 1}{(\beta s + 1)(\lambda s + 1)}}{1 - \frac{\tau^2 s^2 + 2\xi\tau s + 1}{(\beta s + 1)(\lambda s + 1)} \frac{(\beta s + 1)}{(\tau^2 s^2 + 2\xi\tau s + 1)}}$$

$$g_c(s) = \frac{\tau^2 s^2 + 2\xi\tau s + 1}{\lambda s (\beta s + 1)}$$

Comparing with the transfer function of the PID controller,

$$g_c(s) = k_c \left[ \frac{\tau_i \tau_d s^2 + \tau_i s + 1}{\tau_i s} \right]$$

Then from the second order model parameters, the following IMC PID controller tuning formula is used as shown in Table 3.

**Table 3:** IMC PID controller tuning

$\tilde{g}_p(s)$	$f(s)$	$k_c$	$\tau_i$	$\tau_d$
$\frac{(\beta s + 1)}{(\tau^2 s^2 + 2\xi\tau s + 1)}$	$\frac{1}{\lambda s + 1}$	$\frac{2\xi\tau}{\lambda}$	$2\xi\tau$	$\frac{\tau}{2\xi}$

## 4. Results

In this section, the proposed controller design is implemented to the continuous time transfer function of CSTR models to show the efficiency of the proposed controllers.

Firstly, the step response of the open loop CSTR model is shown (Figure 5); secondly the step responses of CSTR model based on conventional PID and IMC based PID controls are shown (Figure 6) and lastly, the Adaptive control step response of the CSTR model is demonstrated (Figures - 7,8,9,10).

### 4.1 Open-loop response of a Jacketed CSTR

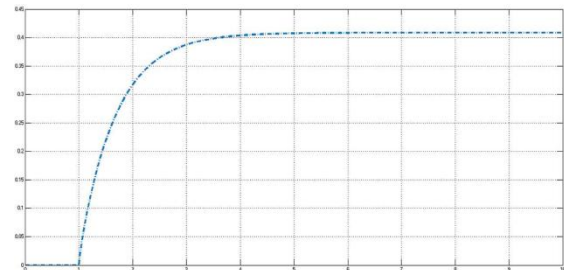


**Figure 5:** Step response of the open loop CSTR model

Figure 5 shows the open loop response of the non-ideal CSTR where x-axis defines the time and y-axis defines the effluent concentration.

### 4.2 Response based on Internal Model Control (IMC)

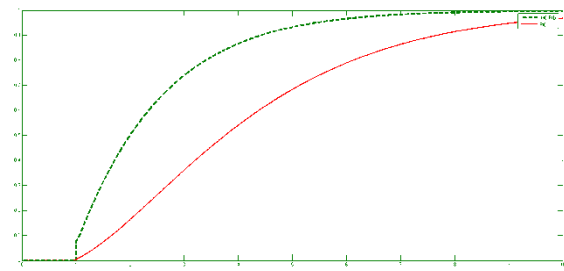


**Figure 6:** Step responses of conventional PID and IMC based PID controller

The simulation results show that the IMC based PID controller has no overshoot and fast response compared to the conventional PID.

### 4.3 Response based on Adaptive control

After obtaining the transfer function of process and the transfer function of the reference model, a MATLAB Simulink model is developed by applying the MIT rule [12].

The following parameters are plotted on the graph: plant output using adaptive control for different values of  $\gamma$ .

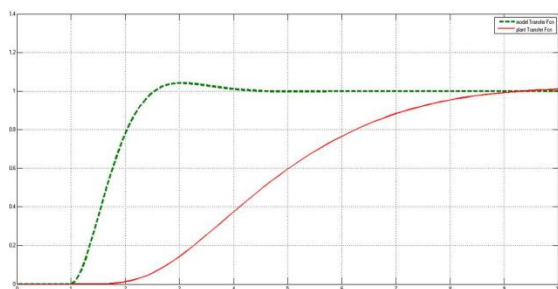


Figure 7: Step response of CSTR based on Adaptive controller when  $\gamma = 0.5$

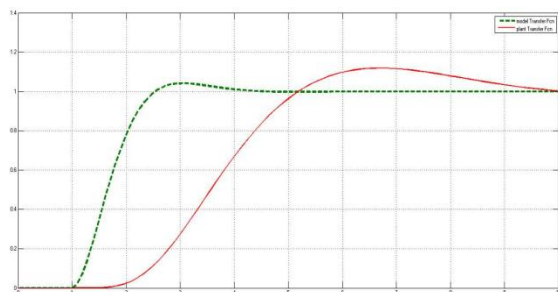


Figure 8: Step response of CSTR based on the adaptive controller when  $\gamma = 1$

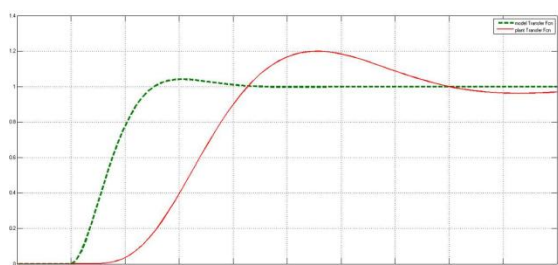


Figure 9: Step response of CSTR based on adaptive controller when  $\gamma = 1.5$

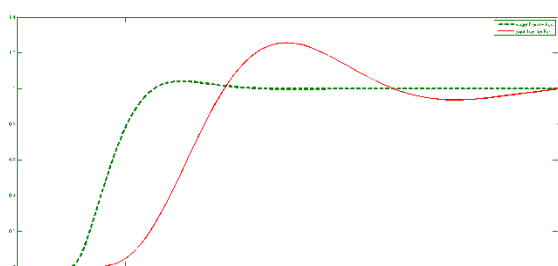


Figure 10: Step response of CSTR based on adaptive controller when  $\gamma = 2$

The effect of adaptive control is analyzed on the time response characteristic of the system. It is observed that with a smaller value of adaption gain the response is very slow. The transient parameters such as settling time, rise time, peak time can be decreased by increasing the value of adaption gain.

Unit step responses of the IMC based PID controller, the conventional PID controller and adaptive controller have been listed in Table 4, which shows that adaptive control requires less

settling time to reach desired steady state and gives less overshoot as compared to the IMC based PID controller and conventional PID controller.

Table 4: Unit step responses of the IMC based PID controller, the conventional PID controller and the adaptive controller

	Settling Time ( $T_s$ )	Rise Time ( $T_r$ )	Peak Time ( $T_p$ )
<b>Conventional PID</b>	$2.8 \times 10^3$	$2.6 \times 10^3$	2948
<b>IMC based PID</b>	513.5	$1.59 \times 10^3$	1742
<b>MRAC with adaptive gain = 0.5</b>	75.94	37.60	85

## 5. Conclusion and Future Scope

The behaviour of the Jacketed CSTR based on adaptive control using MIT rule has been analyzed in this paper. The time response characteristics are observed based on the various adaption gain values. The transient characteristics such as settling time, rise time can be decreased by increasing the adaption gain value. Simulation results of the non-linear model equation of Jacketed CSTR for a first-order irreversible exothermic chemical reaction show that the controller based on adaptive control will give a better response as compared to the IMC based PID controller and conventional PID controller.

The analyzed results and issues during the course of the work give rise to a number of possible directions for future work. Some of them are briefly summarized below:

- (i) Modelling and control of a non-ideal reactor with second-order reaction can be carried out.
- (ii) Tuning of PID can be done using different tuning methodologies such as Cohen-Coon and Artificial Bee-colony based tuning methods, and comparison can be made between the new tuning methods with the proposed control schemes.
- (iii) Modelling can be done by considering Dead space to be a function of time.

## References

[1] S. Deepa, N. Anipriya and R. Subbulakshmy, "Design of Controllers for Continuous Stirred Tank Reactor", *International Journal of Power Electronics and Drive System*

- (*IJPEDS*), Vol. 5, No. 4, April 2015, pp. 576-582. Retrieved from <https://www.researchgate.net/publication/283129558>
- [2] D. E. Seborg, T. F. Edgar, D. A. Mellichamp, F. J. Doyle III, *Process Dynamics and Control*, Third Edition, John Wiley & Sons Inc, NJ, 2011.
- [3] B. W. Bequette, *Process Control: Modelling, Design and Simulation*, Prentice Hall, NJ, 2003.
- [4] M. Gopal, *Digital Control and State Variable Methods: Conventional and Neuro-Fuzzy Control Systems*, 2<sup>nd</sup> Edition, Tata McGraw-Hill Publishing Company Ltd., New Delhi, 2003.
- [5] K. Prabhu and V. M. Bhaskaran, "Optimization of a Control Loop Using Adaptive Method", *International Journal of Engineering and Innovative Technology (IJEIT)*, Vol. 1, Issue 3, March 2012, pp. 133-138. Retrieved from [http://www.ijeit.com/vol%201/Issue%203/IJEIT1412201203\\_29.pdf](http://www.ijeit.com/vol%201/Issue%203/IJEIT1412201203_29.pdf)
- [6] D. E. Rivera and M. E. Flores, "Internal Model Control", in *Control system, Robotics and Automation - Volume II: System Analysis and Control: Classical Approaches-II*, H. Unbehauen (ed.), Vol. 2, pp. 80-108, Eolss Publishers Co. Ltd., Oxford, UK, Oct. 2009.
- [7] N. Kumar and N. Khanduja, "Mathematical modelling and simulation of CSTR using MIT rule", *Proc. of 2012 IEEE 5th India International Conference on Power Electronics (IICPE)*, Delhi, 6-8 Dec. 2012, pp. 1-5. Doi: 10.1109/IICPE.2012.6450458
- [8] R. Aruna and M. S. Kumar, "Adaptive control for interactive thermal process", *Proc. of 2011 International Conference on Emerging Trends in Electrical and Computer Technology*, Nagercoil, 23-24 March 2011, pp. 291-296. Doi: 10.1109/ICETECT.2011.5760131
- [9] K. J. Åström B. and Wittenmark, *Adaptive Control*, 2<sup>nd</sup> Edition, Dover Publications, Inc., NY, Pearson Education, 2013.
- [10] R. Upadhyay and R. Singla, "Application of adaptive control in a process control", *Proc. of 2010 2nd International Conference on Education Technology and Computer (ICETC 2010)*, Shanghai, 2010, pp. V2-323-V2-327. Doi: 10.1109/ICETC.2010.5529373
- [11] C. Adrian, A. Corneliu and B. Mircea, "The simulation of the adaptive systems using the MIT rule", *Proc. of the 10th WSEAS International Conference on Mathematical Methods and Computational Techniques in Electrical Engineering (MMACTEE'08)*, Sofia, Bulgaria, 2-4 May 2008, pp. 301-305. Retrieved from <http://www.wseas.us/e-library/conferences/2008/sofia/MMACTEE/mm-45.pdf>
- [12] N. Khanduja and S. Sharma, "Performance Analysis of CSTR using Adaptive Control", *International Journal of Soft Computing and Engineering (IJSCE)*, Vol. 4, Issue 2, May 2014, pp. 80-84. Retrieved from <https://pdfs.semanticscholar.org/ae42/465453bd4f2fb9af5afde653551e53623377.pdf>
- [13] A. Durgadevi, S. A. Priyadarshini and R. Anbumozhi, "Control of Continuous Stirred Tank Reactor Using Neural Network based Predictive Controller", *Imperial Journal of Interdisciplinary Research (IJIR)*, Vol. 3, Issue 9, pp. 316-321. Retrieved from <https://www.onlinejournal.in/IJIRV3I9/040.pdf>
- [14] T. Jose, R. Antony and S. Isaac, "pH NEUTRALIZATION IN CSTR USING MODELREFERENCE NEURAL NETWORK AND FUZZY LOGIC ADAPTIVE CONTROLLING SCHEMES", *International Journal of Advancements in Research & Technology*, Vol. 2, Issue1, January 2013, pp. 1-6.. Retrieved from <http://www.ijoart.org/docs/pH-NEUTRALIZATION-IN-CSTR-USING-MODELREFERENCE-NEURAL-NETWORK-AND-FUZZY-LOGIC-ADAPTIVE-CONTROLLING-SCHEMES.pdf>

# Optimization of DC Microgrid for Renewable Energy Integration

Risalin Lyngdoh Mairang

Department of Electrical and Electronics Engineering, School of Technology, Assam Don Bosco University, Airport Road, Azara, Guwahati -781017, Assam, INDIA.  
risavecca@gmail.com

**Abstract:** This paper analyses the possibility to develop in optimizing the utilization of renewable energy sources within microgrids. The renewable wind and solar power generation forecast are aggregated, and it is proposed to support the quantification of the operational reserve and maintain the equilibrium of the microgrid’s real-time supply and demand. One potential solution is a microgrid that can be vertically integrated with high-rise buildings which are frequently encountered in urban areas.

**Keywords:** Distributed energy resources, Droop control, State Of Charge (SOC), Microgrid, Multilevel energy storage, Power electronic conversion, Solar power, Wind power.

## 1. Introduction

Renewable energy plays an important role within the society; it is not only increasingly making us more energy dependent, but also creating greater environmental awareness. Once renewable energy technologies have been developed, energy can be produced anywhere. The rooftop generation of renewable energy harvested from wind and solar can be connected to the ground level via a microgrid where the Electric vehicle (EV) charging stations could be supplied. A battery is crucial in this case, to support and maintain the balance of supply and demand. The primary requirement for a DC microgrid operation is to maintain the common DC bus voltage within an acceptable range [2]. According to its optimization, it is proposed to set a droop as a function of the battery’s expected State Of Charge (SOC). The optimization program helps to determine a solution that minimizes the operation cost of the DC microgrid.

When wind and solar energy are combined, it leads to reduced local energy storage management [3]. The combination of battery energy storage system and supercapacitor technologies can form a multilevel energy storage. In this, the battery energy storage system is responsible for balancing the supply and demand, whereas supercapacitor employs cache control to compensate for fast power fluctuations and smoothen the transients encountered by a battery with higher energy capacity. Microgrids or hybrid energy systems have been demonstrated to be an effective structure for local interconnection of distributed renewable generation, loads and storage. Most current microgrid implementations

combine loads with sources, try to use the available waste heat [4].

The battery and the supercapacitor have a better transient response; however, their loss of energy density does not provide enough autonomy to the system. The proposed hybrid energy storage system, having an advanced control system, taking advantage of each storage system and avoiding the cause of degradation and limitation of them, can emerge as the technological solution for the problem commented. The distributed renewable of generation, loads and storage to be an effective structure for local interconnection have been shown in a Microgrid or hybrid energy systems [5-10].

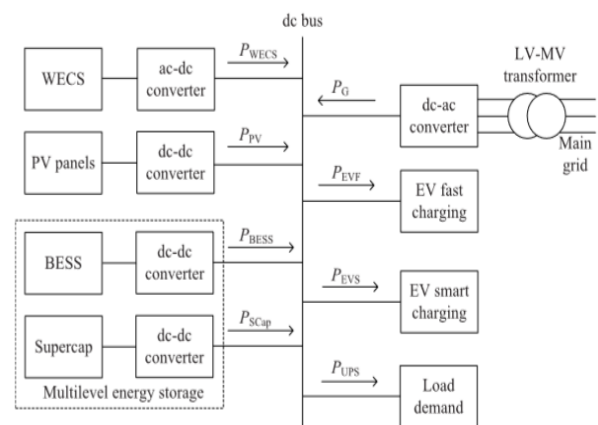


Fig. 1: Layout of a DC microgrid [1]

## 2. Outline of DC Microgrid

A schematic of a DC microgrid is given in Fig. 1, along with the conventions employed for power. The DC bus connects wind energy conversion system (WECS), PV panels, multilevel energy storage comprising of the Battery Energy Storage System (BESS) and the supercapacitor. EV smart charging points, grid interface and EV fast charging station are also connected to the DC bus. The WECS is integrated into the DC bus via AC-DC converter. PV panels are connected to a DC bus through a DC-DC converter.

The BESS can be implemented through flow battery technology connected to the DC bus via a DC-DC converter. The technology that can provide fast and frequent access to stored energy is the supercapacitor [11,12]. The supercapacitor has considerably less energy capacity than the BESS. However, it is used for compensating for fast fluctuations of power and hence it provides cache control as detailed in the research done by K. Strunz and H. Louie [11].

It is connected close to the LV-MV transformer to minimize losses and voltage drop. An LV DC microgrid is well suited for naturally demarcated power systems [13]. For positive values of  $P_G$ , the microgrid takes power from the main grid. For negative values of  $P_G$ , the microgrid supplies power to the main grid. There is a variation in the voltage supply, grid frequency, harmonics, as well as other power quality due to the imbalance of active and reactive power that are introduced in a grid by renewable energies.

H. Kakigano, Y. Miura and T. Ise [12] proposed a low-voltage bipolar-type DC microgrid, which can supply high-quality power. In their work, a system of a residential complex has been represented as the instance of the DC microgrid. In this system, each house has a Co-Generation System (CGS), such as a gas engine or fuel cell.

When the system connects to the utility grid, the deficient power is compensated from the utility grid, but when the system disconnects from the utility grid, the surplus or deficient power is compensated by the energy storages such as a battery and a supercapacitor (Electric Double-Layer Capacitor: EDLC). The main objectives of this paper are to develop new system operation and control methods for the proposed DC microgrid to provide secure and reliable supply to the connected loads.

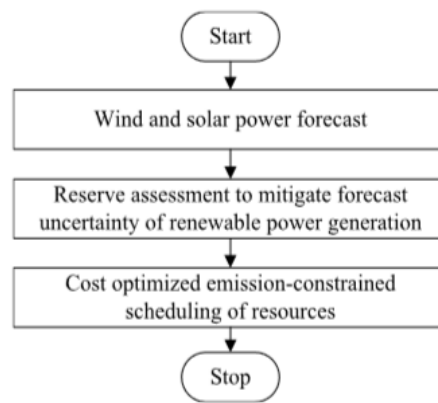


Fig. 2: Overview of Optimized scheduling approach [1]

## 3. Proposed System

The algorithm for optimized scheduling of the microgrid is given in Fig. 2. In the first stage, wind and solar power generations are forecasted. Then, wind and solar power forecast are aggregated to produce the total renewable power forecast model. The aggregated power generation data are utilized to assign hourly positive and negative energy reserves to the BESS for the microgrid operation. The positive energy reserve of the BESS provides the energy stored, which can be readily supplied to the DC bus on demand. The negative energy reserve provides the part of the BESS to remain uncharged to capture access power on demand.

The BESS can only be charged and discharged in the operation area in the normal operation mode, which is scheduled by optimization. The objective of the optimization is to minimize the operating cost of the microgrid in interconnected mode and provide uninterrupted power supply (UPS) service in the autonomous mode. In the interconnected operating mode, an adaptive droop control is devised for the BESS, which is selected based on the deviation between optimize and real-time SOC of the battery.

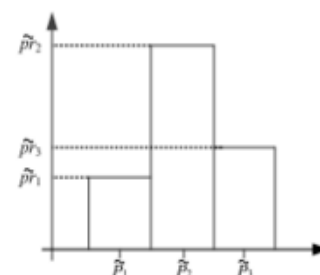


Fig. 3: Wind or solar forecast uncertainty for 1h [1]

## 4. Aggregated Model

The uncertainty of wind and solar power can be presented by a three-state model. The forecast

uncertainty data of the wind and solar power generations are made available for the urban microgrid.

In Fig. 3, the output power state and the probability assigned to that state are available. State 1 represents a power forecast lower than the average power forecast  $\tilde{P}_1$  with the forecast probability of  $\tilde{P}r_1$  assigned to it. The average power forecast and the probability of forecast assigned to it give state 2. State 3 represents a power forecast higher than the average power forecast. Then wind and solar forecasts are aggregated to produce the total renewable power forecast model.

In the three state model  $k = 3$  which is the number of individual states. Table 1 shows that the forecast data of wind and solar generation provided for 1h. For example, at the probability of 50% the wind power will be 50kW.

**Table 1:** Example of Wind and Solar Power Forecast Data

Individual state	State 1	State 2	State 3
Wind forecast	0.25	0.50	0.25
Wind power(kW)	40	50	60
Solar forecast	0.25	0.50	0.25
Solar power(kW)	15	20	25

As the microgrid has two generation resources with three individual states, i.e.  $k = 3$ , then the combined state is  $N = K^2$ , which is equal to 9 in this case. Figure 4, shows the combined states in the forecast uncertainty model of wind and solar power.

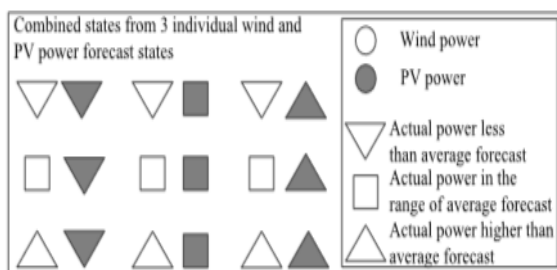


**Fig. 4:** Aggregation of wind and solar power forecast in microgrid [1]

For the wind and solar power forecast shown in Table 1, nine combined states are defined as shown in Table 2. In each of these combined states, the powers of all those individual states are summed up, and the probability of a combined state is equal to the product of the probabilities in individual state, considering the individual states are not correlated.

If an aggregated state  $m$  covers a number of combined states  $L$ , then the probability of having one of those aggregated states is the sum of the probabilities of those combined states.

$$\tilde{p}r_{A,m} = \sum_{l=1}^L \tilde{p}r_{l,m} \dots\dots\dots (1)$$

where,  $\tilde{p}r_{A,m}$  is the forecast probability of renewable power at the aggregated state  $m$ , and  $\tilde{p}r_{l,m}$  is the forecast probability of renewable power at the combines state  $l$  within the aggregated state  $m$ .

$$\tilde{p}A_{,m} = \frac{\sum_{l=1}^L \tilde{p}r_{l,m} \times \tilde{P}_{l,m}}{\tilde{p}r_{l,m}} \dots\dots\dots (2)$$

**Table 2:** Example of Combined States of Wind and Solar Power Forecast

Combined states n	Counter L	Aggregated state m	Power output $\tilde{P}_{l,m}$ (kW)	Probability $\tilde{p}r_{l,m}$
1	1	1	40+15 = 55	0.25×0.25 = 0.0625
2	2	1	40+20 = 60	0.25×0.50 = 0.1250
3	1	2	40+25 = 65	0.25×0.25 = 0.0625
4	2	2	50+15 = 65	0.50×0.25 = 0.1250
5	3	2	50+20 = 70	0.50×0.50 = 0.2500
6	4	2	50+25 = 75	0.50×0.25 = 0.1250
7	5	2	60+15 = 75	0.25×0.25 = 0.6250
8	1	3	60+20 = 80	0.25×0.50 = 0.1250
9	2	3	60+25 = 85	0.25×0.25 = 0.0625

In the example shown in Table 2, employing equations (1) and (2) we get as follows:

$$\tilde{p}r_{A,1} = 0.0625 + 0.1250 = 0.1875$$

$$\begin{aligned} \tilde{p}A_{,1} &= \frac{55 \times 0.0625 + 60 \times 0.1250}{0.1875} \text{ kW} \\ &= 58.33 \text{ kW} \end{aligned}$$

A summary of the aggregated three-state model for renewable power generation is provided in Table 3.

**Table 3:** Aggregated Three State Power Forecast Model for 1h

Aggregated state $M$	1	2	3
Probability $\tilde{p}r_{A,m}$	0.1875	0.6250	0.1875
Power output $\tilde{P}_{A,m}$ (kW)	58.33	70	81.67

### 5. Existing System

The researchers L. Roggia *et al.* [15], proposed a novel integrated converter topology for interfacing between the energy storage system and the DC bus for a residential microgrid application. The proposed DC-DC converter is the integration of the full-bridge and a forward converter. Full-bridge converter is in the authority of the energy storage system discharging stage, whereas the forward converter is liable for the energy storage system charging stage.

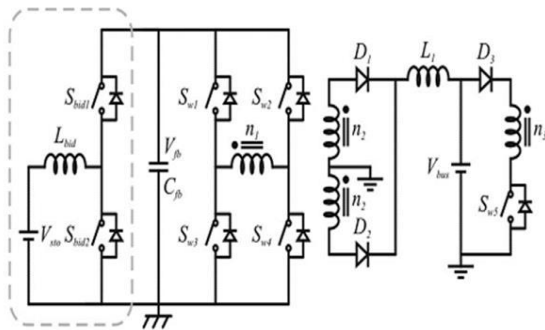


**Fig. 3:** Proposed integrated full-bridge-forward DC-DC converter including bidirectional converter [15]

During discharging stage of the energy storage system, the bidirectional converter boosts the voltage from the energy storage system to an intermediate level, whereas during the energy storage system’s charging stage, it performs voltage post regulation or remains with  $S_{bid1}$  ON and  $S_{bid2}$  OFF acting as a low-pass filter, thus it eliminates the switching losses. A three-winding transformer is required in this topology as proposed by the researchers L. Roggia *et al.* [15]. Windings 1 and 2 are used in the full-bridge operation, and windings 1 and 3 are in the forward operation. One diode is required to be added in series with the transformer tertiary winding to avoid any current circulation via the antiparallel diode of the forward converter switch during the full-bridge converter operating mode.

### 6. Adaptive Droop Control

Adaptive droop control is devised for the BESS in the interconnected mode of operation, while the BESS is for keeping the voltage of a DC bus in a

defined acceptable range for providing UPS service in term of an autonomous mode of operation [1].

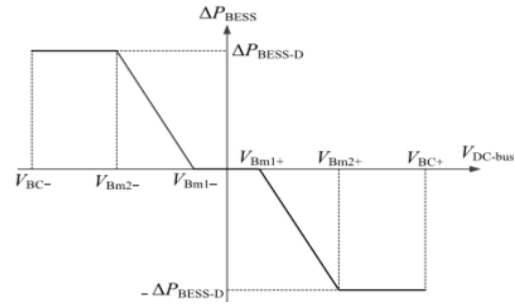


**Fig. 3:** The Droop control of a BESS power electronic converter to mitigate power deviations of DC microgrid in normal condition of the BESS [1]

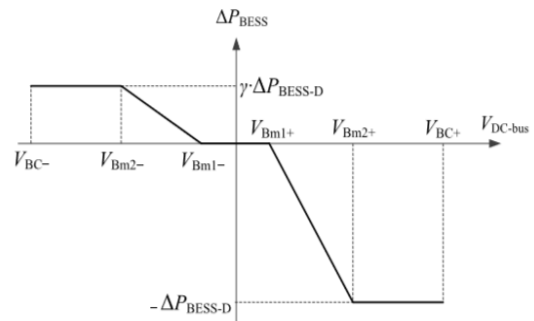


**Fig. 4:** Droop control of BESS power electronic converter to mitigate the power deviations of DC microgrid is lower than the schedules SOC of the BESS [1]

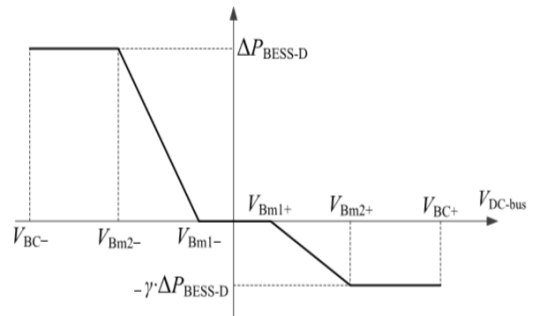


**Fig. 5:** Droop control of the BESS to mitigate the power deviations of DC microgrid in higher than the scheduled SOC of the BESS [1]

The second droop curve, as shown in Fig. 4, is devised for a situation in which the real-time SOC of the BESS is less than the optimized and scheduled SOC of the BESS. Thus, the BESS is contributing to stabilize the DC bus voltage by charging at the same power as shown in Fig. 3. This way, the SOC is capable of coming closer to the optimized and scheduled SOC.

The third droop as shown in Fig. 5 is devised for a situation where the real-time SOC of

the BESS is higher than the optimized and scheduled SOC of the BESS. So, the BESS contributes to stabilizing the DC bus voltage by discharging at the same power as shown in Fig. 3.

### 7. Comparison of Results

A comparison of the results (as below) shows the importance of coordinating the droop settings with scheduling in microgrids with wind and solar power.

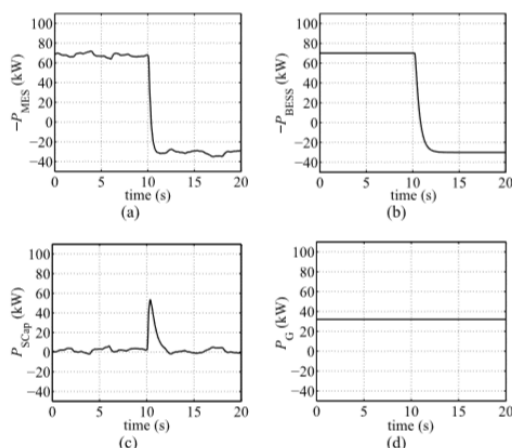


**Fig. 6:** Case A: Droop-control-based responses to wind fluctuation and fast charging when SOC of the battery is as scheduled: (a) Multilevel energy storage system (MES) charging power from the DC bus, (b) Battery charging power from the DC bus, (c) Supercapacitor discharging power to the DC bus, (d) Grid power to the DC bus [1]

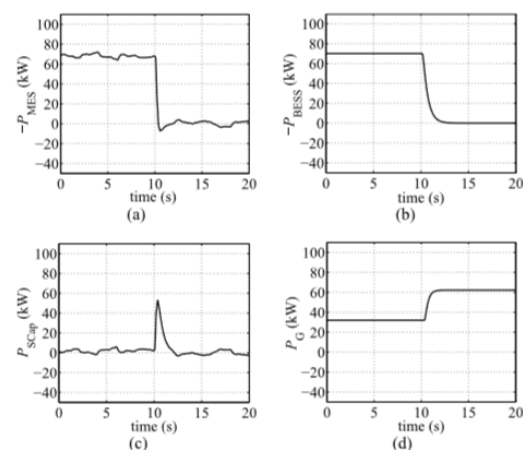


**Fig. 7:** Case B: Droop-control-based responses to wind fluctuation and fast charging when SOC of the battery is lower than the scheduled: (a) Multilevel energy storage system (MES) charging power from the DC bus, (b) Battery charging power from the DC bus, (c) Supercapacitor discharging power to the DC bus, (d) Grid power to the DC bus [1]

In Case A, SOC of the battery is assumed to be within the close range of the scheduled SOC, while resulting from the day ahead optimization. The simulation result of the control shown in Fig. 3 is given in Fig. 6.

In Case B, the BESS is assumed to have lower than the expected SOC compared with SOC scheduled in optimization. The simulation result of the control shown in Fig. 4 is given in Fig. 7. With the asymmetric curve of the BESS (Fig. 4), the multilevel energy storage does not provide full compensation of renewable fluctuation. Hence, droop control of the grid is activated; and from the main grid, it contributes the power demand to the fast charging.

The SOC of the battery, shown in Fig. 6, is as desired according to the scheduling, while the SOC of the battery becomes lower than the expected due to forecast uncertainty as shown in Fig. 7. In the latter case, the asymmetric droop as shown in Fig. 4, avoids further significant discharging but has full droop contribution on the charging side. On the reduced discharging side, the droop on the other power electronic converter connects to the main grid.

### 8. Conclusion

A DC microgrid for optimization of renewable power integration has been proposed. The operational optimization and power electronic based voltage-power droop control were developed. Microgrids are beneficial for the development of efficient and cost-effective energy storage technology.

The battery can be connected in parallel with a supercapacitor to form a multilevel energy storage. The battery plays an important role in compensating renewable power fluctuations and providing the power needed. The optimization for power exchanges and DC voltage control by using adaptive control are normally done through power electronic converters.

Nowadays, natural energy stored in fossil fuels is coming to its end. This fact will globally change the way our society manages energy. So for future developments will be based on expanding the technique into developing an optimal control algorithm of renewable energy microgrid with photovoltaic generator and wind turbine.

The usage of wind and solar energy reduces emission, free from pollution and so on, which is convenient for the citizen and resulting energy system serves local stationary, and it is a good citizen within the main grid.

## References

- [1] K. Strunz, E. Abbasi and D. N. Huu, "DC Microgrid for Wind and Solar Power Integration", *IEEE Journal of Emerging and Selected Topics in Power Electronics*, Vol. 2, Issue 1, March 2014, pp. 115-126. Doi: 10.1109/JESTPE.2013.2294738
- [2] D. Chen, L. Xu and L. Yao, "DC Voltage Variation Based Autonomous Control of DC Microgrids", *IEEE Transactions on Power Delivery*, Vol. 28, Issue 2, April 2013, pp. 637-648. Doi: 10.1109/TPWRD.2013.2241083
- [3] B. S. Borowy and Z. M. Salameh, "Methodology for optimally sizing the combination of a battery bank and PV array in a wind/PV hybrid system", *IEEE Transactions on Energy Conversion*, Vol. 11, Issue 2, June 1996, pp. 367-375. Doi: 10.1109/60.507648
- [4] R. H. Lasseter and P. Paigi, "Microgrid: A Conceptual Solution," *Proc. of 2004 IEEE 35th Annual Power Electronics Specialists Conference (IEEE Cat. No.04CH37551)*, Vol. 6, Aachen, Germany, 20-25 June, 2004, pp. 4285-4290. Doi: 10.1109/PESC.2004.1354758
- [5] A. L. Dimeas and N. D. Hatziargyriou, "Operation of a multiagent system for microgrid control", *IEEE Transactions on Power Systems*, Vol. 20, Issue 3, Aug. 2005, pp. 1447-1455. Doi: 10.1109/TPWRS.2005.852060
- [6] F. Katiraei and M. R. Iravani, "Power Management Strategies for a Microgrid With Multiple Distributed Generation Units", *IEEE Transactions on Power Systems*, Vol. 21, Issue 4, Nov. 2006, pp. 1821-1831. Doi: 10.1109/TPWRS.2006.879260
- [7] A. G. Madureira and J. A. P. Lopes, "Coordinated voltage support in distribution networks with distributed generation and microgrids", *IET Renewable Power Generation*, Vol. 3, Issue 4, Dec. 2009, pp. 439-454. Retrieved from <https://repositorio.inesctec.pt/bitstream/123456789/1646/1/PS-06074.pdf>
- [8] M. H. Nehrir, C. Wang, K. Strunz, H. Aki, R. Ramakumar, J. Bing, Z. Miao and Z. Salameh, "A Review of Hybrid Renewable/Alternative Energy Systems for Electric Power Generation: Configurations, Control, and Applications", *IEEE Transactions on Sustainable Energy*, Vol. 2, Issue 4, Oct. 2011, pp. 392-403. Doi: 10.1109/TSTE.2011.2157540
- [9] R. Majumder, B. Chaudhuri, A. Ghosh, R. Majumder, G. Ledwich and F. Zare, "Improvement of Stability and Load Sharing in an Autonomous Microgrid Using Supplementary Droop Control Loop", *IEEE Transactions on Power Systems*, Vol. 25, Issue 2, May 2010, pp. 796-808. Doi: 10.1109/TPWRS.2009.2032049
- [10] D. Westermann, S. Nicolai and P. Bretschneider, "Energy management for distribution networks with storage systems — A hierarchical approach", *Proc. of 2008 IEEE Power and Energy Society General Meeting - Conversion and Delivery of Electrical Energy in the 21st Century*, Pittsburgh, PA, 20-24 July 2008, pp. 1-6. Doi: 10.1109/PES.2008.4596533
- [11] K. Strunz and H. Louie, "Cache Energy Control for Storage: Power System Integration and Education Based on Analogies Derived From Computer Engineering", *IEEE Transactions on Power Systems*, Vol. 24, Issue 1, Feb. 2009, pp. 12-19. Doi: 10.1109/TPWRS.2008.2005713
- [12] H. Kakigano, Y. Miura and T. Ise, "Low-Voltage Bipolar-Type DC Microgrid for Super High Quality Distribution", *IEEE Transactions on Power Electronics*, Vol. 25, Issue 12, Dec. 2010, pp. 3066-3075. Doi: 10.1109/TPEL.2010.2077682
- [13] D. Salomonsson, L. Soder and A. Sannino, "Protection of Low-Voltage DC Microgrids", *IEEE Transactions on Power Delivery*, Vol. 24, Issue 3, July 2009, pp. 1045-1053. Doi: 10.1109/TPWRD.2009.2016622
- [14] L. Xu and D. Chen, "Control and Operation of a DC Microgrid With Variable Generation and Energy Storage", *IEEE Transactions on Power Delivery*, Vol. 26, Issue 4, Oct. 2011, pp. 2513-2522. Doi: 10.1109/TPWRD.2011.2158456
- [15] L. Roggia, L. Schuch, J. E. Baggio, C. Rech and J. R. Pinheiro, "Integrated Full-Bridge-Forward DC-DC Converter for a Residential Microgrid Application", *IEEE Transactions on Power Electronics*, Vol. 28, Issue 4, April 2013, pp. 1728-1740. Doi: 10.1109/TPEL.2012.2214061

# Electrical Methods of Soil Moisture Measurement: A Review

Muktimani Brahma<sup>1</sup>, Bikramjit Goswami<sup>2</sup>

<sup>1,2</sup> Department of Electrical and Electronics Engineering, School of Technology, Assam Don Bosco University,  
Airport Road, Azara, Guwahati -781017, Assam, INDIA.

<sup>1</sup>mukti33@gmail.com, <sup>2</sup>bikramjit.goswami@dbuniversity.ac.in\*

**Abstract:** Soil moisture is an important factor that is of immense importance in the field of engineering, agriculture and ecology. The permittivity of soil is dependent on the water level present in the soil. Development of weather patterns and the production of precipitation depend on soil moisture. A number of soil moisture measurement techniques are being developed by various researchers. This paper reviews the various electrical methods of measuring soil moisture, such as the dielectric method, electrical resistance method and electrical capacitance method.

**Keywords:** Soil moisture, electrical methods to measure soil moisture, Irrigation, Resistivity of soil, Resistivity probe.

## 1. Introduction

Soil moisture is the water content in the soil. The permittivity of the soil is dependent on the water level present in the soil. Development of weather patterns and the production of precipitation depend on soil moisture [1]. Measurement of soil moisture is important for irrigation schedules. By measuring the soil water content, soil moisture can be determined.

Soil moisture is important for the plant's growth. Moist soil increases the rate of diffusion because soil water is the pathway for ion movement and thickness of water film determines the ease of nutrient movement to the root [2]. Thus, it is important to keep the soil moist to the desired level for healthy crops. Soil moisture content is measured using different electrical techniques.

## 2. Electrical Methods of Soil Moisture Measurement

The following techniques employ the electrical properties of the soil to measure the moisture content in the soil: Electrical resistivity and dielectric constant.

### 2.1 Electrical Resistivity Technique

The principle of electrical measurement of soil moisture was first reported by Whitney *et al.* in 1897 [2]. Electrical resistance technique operates on the principle that resistance between two electrodes immersed in the soil will depend on the moisture content of the soil [2]. Later, J. A. Munoz *et al.* [3] observed the electrical resistivity of

natural unsaturated loess, a loosely compacted yellowish-grey deposit of wind-blown sediment. Cylindrical specimens were extracted from the ground for that purpose. The system used a precision balance to measure the change in water mass, of a metallic cylindrical mould housing the specimen of a plastic cover disk accommodating the resistivity probe as well as covering the specimen to avoid evaporation at the time of measurement. The electrical resistivity probe was used for measuring the resistivity of soil with variation in moisture. The volumetric water content increased from 5.8% to 38.5% with a decrease in resistivity from 338  $\Omega$ -m to 8  $\Omega$ -m. For dry soil, the resistivity reached values higher than 50  $\Omega$ -m. At lowest degrees of saturation, resistivity is highest and vice versa.

Sudhir *et al.* [4] used electrical resistivity method for determining the water content in the sand. Figure 1 shows the setup for measuring the electrical resistivity of sand. The oven dried sand and bore well water was used for preparing the sample. The predefined water quantity is added to sand and kept in plastic bags for 24 hours in a PVC mould in 3 layers. The mould is cylindrical, and the ends are pressed with copper plates, which behave as the outer electrodes. Two other copper rods were placed inside the specimen with a spacing of 0.0424 m. DC voltage ranging from 0 to 30V is applied to the outer plates, and the resistivity is measured. One 2K resistance is inserted in series with the specimen to measure the current. At a low water content of 1.02%, the resistivity is undetermined. For 30V DC supply, electrical resistivity value varied between 49.723 to 297.666  $\Omega$ -m and the mean is 140.913. The analysis showed

that the ER increases with a decrease in moisture content.

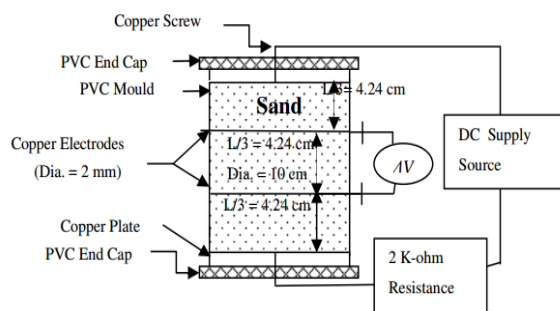


**Figure 1:** Setup for measuring electrical resistivity of sand [4]

Soil sample extracted from the field may not have the same resistivity as that of the field because of their degree of compaction. However, the moisture content in them would remain the same, if kept in a sealed container. W. John McCarter [5] found the electrical resistivity characteristics for compacted clays. Figure 2 shown below is the setup for measuring the resistance of the compacted clay.

The sample was compressed into a conductivity cell. The electrical resistance is measured by Terrameter. The two-electrode model of electrical resistivity measurement is used over the four-electrode model as it nullifies the uncertainty over the cross-sectional area and electrode sample coupling. After testing, the clay is remixed and compacted to ensure the moisture remains constant. At saturation, the moisture content remained constant. The resistivity dropped as the volumetric water content is zero and increasing the same showed change in resistivity. Similarly, it has been observed that increasing the degree of saturation also decreases the resistivity. Resistivity is thus a function of moisture content and degree of saturation.

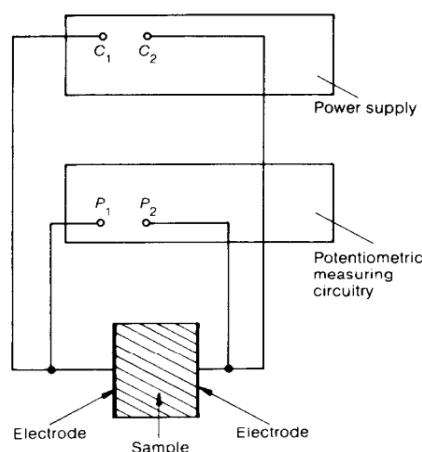


**Figure 2:** Schematic diagram of sample resistance measurement [5]

The soil water content of maize farm with sandy loam soil is investigated using a vertical sounding technique [11]. The electrodes used were made of copper wires supported by wood. Copper wires are the conducting medium and wood supported wires in the ground. The electrodes were connected to 40m long cable with an electrode separation of 0.2m. The electrodes are inserted into the ground close to the plants. The jumpers connected to the copper part of electrodes through cable take-outs are connected to WWEN32S protocol. The resistivity obtained was in the range of 40-60 Ω-m for the sandy loam soil.

A clear relationship exists between the soil moisture and soil resistivity, which makes the electrical resistivity method simple and reliable.

## 2.2 Dielectric Technique

Time Domain Reflectometry (TDR), capacitance technique and Frequency Domain Reflectometry (FDR) are the techniques that use the dielectric property of the soil for measuring soil moisture content.

### 2.2.1 Time Domain Reflectometry (TDR)

The apparent dielectric constant is measured by measuring within the time region the round trip rate of electromagnetic waves at a constant frequency (a high frequency from 30 MHz to 3 GHz) to and from metal electrodes buried in the soil. The cable tester produces high-frequency electromagnetic pulses and monitors reflected waves, rods inserted into the soil, the cable connecting the tester and rods. [6].

Spatial variations play a key role in the Terroir effect. Terroir effect involves the environmental factors affecting a crop's epigenetic qualities. Spatial variation in soil water is barely considered while measuring with TDR. TDR measures a small volume of soil, so no information of lateral spatialization is observed [7].

### 2.2.2 Capacitance Technique

The moisture content can be measured by measuring the dielectric constant, which can be measured by capacitance. The dielectric constant of water is 81 (approx.), 3 to 5 (approx.) for dry soil, and 1 (approx.) for air. The capacitance method is used for measuring the moisture content of soil; because, the dielectric constant increases with an increase in the water content. Capacitance,  $C$  is directly proportional to the dielectric constant,  $K_d$ .

$$C = G_C K_d$$

Where  $G_c$  represents the shape factor that is dependent on the size and shape of the capacitance sensor and the distance between the electrodes [6]. Figure 3 below shows the schematic diagram of soil moisture measurement using capacitance method. The capacitance sensor consists of two electrodes, which are to be immersed in the soil. The two electrodes form the capacitor and soil act as the dielectric material. Change in the frequency of the oscillator indicates a change in soil moisture [10].

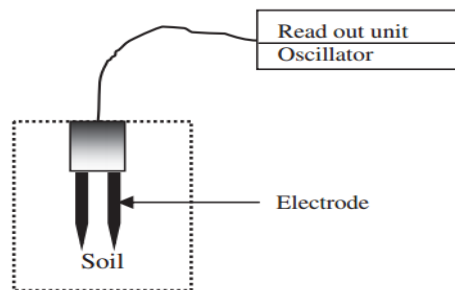


**Figure 3:** Schematic diagram of soil moisture measurement using capacitance technique [10]

T. J. Dean *et al.* [8] used the bridge method with 30 MHz, which required manual balance to measure the dielectric constant. The probe is directly inserted into the soil surface layers. The calibration is done by the gravimetric method. The sensor inserted in the access tube measures the capacitance of the electrodes with a dielectric comprising of moist soil surrounding the access tube. Aluminium probes are installed to minimize the soil disturbance and possibility of air gap around the access tube. For a capacitance probe, the air gap is significant because of its sensitivity. For that purpose, a steel rod was used to set up an annular gap tapering. Thus, the technique can tolerate air gaps while installing the access tube without prejudice to accuracy.

Measurement of frequency is one of the factors affecting the sensitivity of the capacitance sensor measurement. Kizito *et al.* [9] constructed a moisture probe with 5.2 cm long pongs. Sensor performance was obtained by partial vertical immersion of sensor pongs in known salt solutions. The sensitivity of the probe with changing salinity decreased with the increase in frequency. Further increase in frequency did not reduce the sensitivity any further.

### 2.2.3 Frequency Domain Reflectometry (FDR)

FDR measures the interference waves produced when electromagnetic waves emitted on continuous frequencies (100 MHz to 1.7 GHz) in the frequency region as they complete a round trip

at the sensor rod inserted in the soil, allowing the determination of the dielectric constant from peak features [6]. Figure 4 shows the schematic diagram of FDR for soil moisture measurement. The FDR has the same working principle as that of the Capacitance Technique.

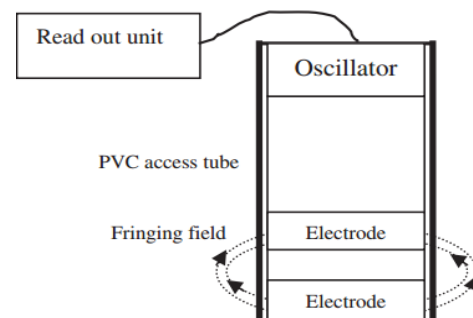


**Figure 4:** Schematic diagram for soil moisture measurement using FDR [10].

FDR probe is better in soils having volumetric moisture content lesser than 5% and hence, its sensitivity is high for volumetric moisture content measurement in relatively dry soil. Earlier researches showed that FDR probe shows erroneous results, being sensitive to air gaps between soil, the access tube and the probe [10].

## 3. Conclusion

The researchers have developed various electrical techniques viz., Electrical Resistivity (ER) technique, the capacitance technique, FDR, TDR for measuring soil moisture. Electrical Resistivity technique is used for spatial measurement of soil water. For monitoring soil water content by ER technique, calibration can be performed both in the field and in the laboratory. The TDR and electrical resistivity method can be used in the field to find ER and Soil Moisture relationship. The soil moisture results will be different for different techniques depending on the factors like salinity, soil type, temperature etc.

## References

- [1] "Soil Moisture", *Marshall Space Flight Center Earth Science Office, NASA*, Dec. 30, 1999. [Online]. Available: <https://weather.msfc.nasa.gov/landprocess/> (Accessed: 12 Feb. 2017)
- [2] A. I. Johnson, "Methods of Measuring Soil Moisture in the Field", *Geological Survey Water-Supply Paper 1619-U, Contributions To The Hydrology of The United States*, U.S. Department of The Interior, U.S. Geological Survey, U.S. Government Printing Office,

- Washington, 1962. Retrieved from <https://pubs.usgs.gov/wsp/1619u/report.pdf>
- [3] J. A. Muñoz-Castelblanco, J. M. Pereira, P. Delage and Y. J. Cui, "The Influence of Changes in Water Content on the Electrical Resistivity of a Natural Unsaturated Loess", *Geotechnical Testing Journal*, Vol. 35, Issue 1, 2012, pp. 11-17. Doi: <https://doi.org/10.1520/GTJ103587>
- [4] S. Bhatt and P. K. Jain, "Correlation between electrical resistivity and water content of sand - a statistical approach", *American International Journal of Research in Science, Technology, Engineering & Mathematics (AIJRSTEM)*, Vol. 6, Issue 2, 2014, pp. 115-121. Retrieved from <http://iasir.net/AIJRSTEMpapers/AIJRSTEM14-342.pdf>
- [5] W. J. McCarter, "The electrical resistivity characteristics of compacted clays", *Geotechnique*, Vol. 34, Issue 2, June 1984, pp. 263-267. Retrieved from <https://www.researchgate.net/publication/245410154>
- [6] M. Inoue and T. Shimizu, "Experimental Set-up to Continuously Monitor Water Flow and Solute Transport in Unsaturated Large Weighing Lysimeters", *Research Paper in Annual Report of Arid Land Research Center, Tottori University*, 1997, pp. 1-14. Retrieved from <https://www.alrc.tottori-u.ac.jp/english/achievements/annual/1997-1998/paper.pdf>
- [7] L. Brillante, O. Mathieu, B. Bois, C. van Leeuwen and J. Lévêque, "The use of soil electrical resistivity to monitor plant and soil water relationships in vineyards", *Soil*, Vol. 1, March 2015, pp. 273-286. Doi: <https://doi.org/10.5194/soil-1-273-2015>
- [8] T. J. Dean, J. P. Bell and A. J. B. Baty, "Soil moisture measurement by an improved capacitance technique, Part I. Sensor design and performance", *Journal of Hydrology*, Vol. 93, Issues 1-2, 1987, pp. 67-78. Doi: [https://doi.org/10.1016/0022-1694\(87\)90194-6](https://doi.org/10.1016/0022-1694(87)90194-6)
- [9] F. Kizito, C. S. Campbell, G. S. Campbell, D. R. Cobos, B. L. Teare, B. Carter and J. W. Hopmans, "Frequency, electrical conductivity and temperature analysis of a low-cost capacitance soil moisture sensor", *Journal of Hydrology*, Vol. 352, Issues 3-4, May 2008, pp. 367-378. Doi: <https://doi.org/10.1016/j.jhydrol.2008.01.021>
- [10] S. Lekshmi S. U., D. N. Singh and M. S. Baghini, "A critical review of soil moisture measurement", *Measurement*, Vol. 54, August 2014, pp. 92-105. Doi: <https://doi.org/10.1016/j.measurement.2014.04.007>
- [11] I. S. Jakalia, A. A. Aning, K. Preko, N. Sackey and S. K. Danuor, "Implications Of Soil Resistivity Measurements Using The Electrical Resistivity Method: A Case Study Of A Maize Farm Under Different Soil Preparation Modes At KNUST Agricultural Research Station, Kumasi", *International Journal of Scientific & Technology Research*, Vol. 4, Issue 1, January 2015, pp. 9-18. Retrieved from <https://www.researchgate.net/publication/306264655>

# A Review On Light Trapping Capacities of Different Photovoltaic Cells

Nayanjyoti Deka<sup>1</sup>, Papul Changmai<sup>2</sup>

<sup>1,2</sup> Department of Electrical and Electronics Engineering, School of Technology, Assam Don Bosco University,  
Airport Road, Azara, Guwahati -781017, Assam, INDIA.

<sup>1</sup>njdtrade@gmail.com\*, <sup>2</sup>papuljec5@gmail.com

**Abstract:** *As human beings mostly depend on fossil fuels for all of their daily energy usages. But due to the exponential increase in the graph of the price of the fossil fuels, as well as the gradually decreasing graph of their availability on a large scale, makes the people to divert their attention towards a new source of sustainable energy which could fulfil their daily energy needs reliably, efficiently as well as cost-effectively. Among all renewable sources, the solar energy is an energy source whose availability is free and in an enormous amount; but the main thing is that steps should be undertaken in order to harness the solar energy properly. The following contents in the paper are based on the ways that how solar energy could be harnessed profitably.*

**Keywords:** Light Absorption, Solar Efficiency, Amorphous silicon, Light trapping.

## 1. Introduction

Solar energy is free from pollution and noise; thus a clean source of energy [2]. PV systems are easy to get installed and are long lasting while the cost of maintenance and operation are minimal [1]. Also, it has no parts that move when oriented in a particular angle, so no fear of breakage [11]. Thus the abundant or inexhaustible [11] nature of solar rays and its reliable operation as well its non-degrading nature without any public fear; leads to its prime worthiness. Efficiency, reliability, and cost are the basic parameters, which acts as a wheel for its success commercially [3]. The visible range of the solar rays contains the highest energy density, that is why, whatever the solar cell type is, it is designed in such a way that the cell performs better by absorbing the sunlight properly in the visible range. Sunlight is composed of (i) Direct or beam radiation- sunlight received by the surface of the earth, (ii) Diffuse radiation- also called scattered sunlight, and (iii) Albedo radiation- the reflected sunlight from the ground. The sum of these three components of light is called global radiation. When this global radiation enters the atmosphere of the earth, the molecules that are present in the atmosphere faces three situations, i.e. absorption of the light, scattering of the light and passing of the light unaffected. The ozone layer of the atmosphere absorbs the ultraviolet (UV) region of the sunlight; along with that CO<sub>2</sub> is absorbed by visible region and water vapour particles are absorbed by the infrared region. The best advantage of the photovoltaic (PV) panels is that they are able to absorb both the direct and diffuse irradiations, as a result of which PV panels functions even on

cloudy days [7]. The standard condition for testing a solar cell during its designing is under the Standard Test Conditions: Air Mass 1.5 (AM1.5). It specifies a module temperature of 25°C, an irradiance of 1000 W/ m<sup>2</sup> with an air mass 1.5 (AM1.5) spectrum and zero wind speed. Going back to its history then we got that in 1839, Alexandre Edward Becquerel was the first person to discover the Photovoltaic cells, which are based on the photovoltaic effect. He found it while experimenting with an electrolytic cell that certain materials are there which generates a little amount of current when it is exposed to the light. But, he did not provide any details regarding the factors based on which the electron's generation from an irradiated metal varied by changing the wavelength of light. Then Albert Einstein in 1905, based on his research described the photovoltaic effect as nothing but the photoelectric effect, which means that light acts as a particulate matter. Later, Russel Ohl in 1946, invented the first modern solar cell made of silicon [2].

## 1. Solar Cell Basics (PN Junction)

To construct a solar cell, a p-n junction is required in semiconductors, which is created through dopants. A p-n junction cannot be made just by placing a p-type and an n-type semiconductor in close contact with each other because at the atomic level, at their junctions the continuous contact is not possible; that's why both the acceptor and donor impurity must be grown on the same crystal. The 'n-type' side of a semiconductor has dopants from either group a V or VI column materials of the periodic table with one electron, that it wants to

remove from the valence band to the conduction band; and the ‘p-type’ side of a semiconductor has dopants from either group II or III column materials in the periodic table, that want to accumulate an electron. In n-type, electrons are the major charge carriers and holes are minor charge carriers; but in p-type it is totally opposite to that of the n-type. But, whatever be the level or type of doping, the doping does not disturb the overall charge neutrality of the semiconductor. Along with that, as long as the lattice structure remains the same, the rate of recombination, as well as the rate of generation, remains the same. Also, further we see the energy band or band gap energy (E.g., 1.17 for Silicon (Si) and 0.74 for Germanium (Ge)), which is comprised of enormously large number of energy levels which are closely spaced within a very small range of energy. Then, there is the Fermi energy, i.e., the energy level corresponding to the Fermi level, which is defined as the highest energy level in the conduction band filled up with electrons at absolute zero temperature. When we see the p-n junction, we get a small portion of the junction, which is devoid of any free charge carriers or what we call it as “immobile ions region”; this portion is called depletion layer [4].

The process of solar energy conversion is explained with the help of Figure 1 below.

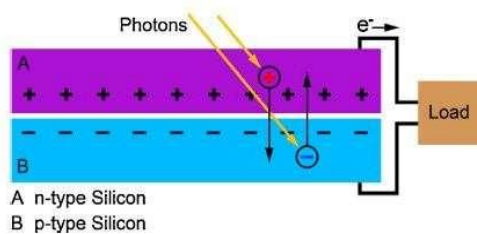


**Figure 1:** operation of a PN device [22]

When light or photon energy hits the semiconductor, and the incident light has the energy equal to the band gap energy then it extracts an electron from the valence band to conduction band. But if less, then it does not extract. Also, there is an important point that if the incident photon has energy more than the band gap energy, it will extract an electron; but along with that, it releases the extra amount of energy as heat which is a loss to the system. Thus, there is an electron in the conduction band and a hole is created in the valence band. Now, when the semiconductor is connected across an external load, the mobile electron moves through the external circuit to the load and in turn, again comes back to the valence band to fill up the hole created earlier; and in that way, again an electron moves to the conduction band. In this way, the flow goes on [22].

## 2. Solar Cell Characteristic Equations

Solar Cell I-V Characteristic Curves show the current and voltage (I-V) characteristics of a particular photovoltaic (PV) cell, module or array giving a detailed description of its solar energy conversion ability and efficiency. Knowing the electrical I-V characteristics (more importantly  $P_{max}$ ) of a solar cell, or panel is critical in determining the device’s output performance and solar efficiency. Solar cells produce direct current (DC) electricity and current times voltage equals power so that we can create solar cell I-V curves representing the current versus the voltage for a photovoltaic device. Solar Cell I-V Characteristics Curves are a graphical representation of the operation of a solar cell or module summarising the relationship between the current and voltage at the existing conditions of irradiance and temperature. I-V curves provide the information required to configure a solar system so that it can operate as close to its optimal peak power point (MPP) as possible. Solar Cell I-V Characteristic Curves are graphs of output voltage versus current for different levels of insolation and temperature and can tell us a lot about a PV cell or panel’s ability to convert sunlight into electricity. The most important values for calculating a particular panel’s power rating are the voltage and current at maximum power.

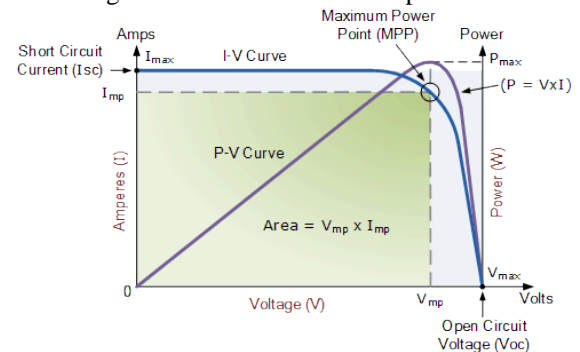


**Figure 2:** Solar Cell I-V Characteristic Curve

Figure 2 shows the I-V characteristics of a typical silicon PV cell operating under normal conditions.

The I-V characteristic equation for solar cell is as mentioned in eqn. (1):

$$I = I_L - I_0 \left( e^{\frac{qV}{nkT}} - 1 \right) \dots\dots\dots (1)$$

Where  $I_L$  is the light generated or load current;  $I_0$  is dark saturation current (depends on the recombination of the solar cell)

$q = 1.6 \times 10^{-19}$  C (q is the charge of an electron)

$k$  (Boltzmann constant) =  $1.38 \times 10^{-23}$  J / Kelvin

The cell current at various irradiance levels can be expressed as in eqn. (2):

$$I(G) = \left(\frac{G}{G_0}\right) I(G_0) \dots\dots\dots (2)$$

Where,  $G_0$  (photogeneration rate) = 1 kW/m<sup>2</sup> at AM1.5

The power extracted from a PV cell is as mentioned in eqn. (3):

$$P_{cell} = V_{cell} \times I_{cell} \dots\dots\dots (3)$$

The open circuit voltage ( $V_{oc}$ ) is logarithmically dependent on the cell illumination level and the short circuit current ( $I_{sc}$ ) is linearly dependent on the cell illumination level.  $V_{oc}$ , i.e. the maximum voltage available from a solar cell, occurs when no current is flowing through the solar cell.  $I_{sc}$ , i.e. the maximum current flows through the solar cell, when the voltage is not present across the solar cell (i.e., short-circuited cell).

$V_{oc}$  (measures the amount of recombination) can be expressed as in eqn. (4):

$$V_{oc} = \left(\frac{nkT}{q}\right) \times \ln\left(\frac{I_L}{I_o} + 1\right) \dots\dots\dots (4)$$

where ‘ $n$ ’ is the ideality factor and it is the measure of how closely the diode obeys the ideal diode equation.

The short-circuit current  $I_{sc}$  (due to collection and generation of light carrying charges) is expressed as in eqn. (5):

$$I_{sc} = qG(L_n + L_p) \dots\dots\dots (5)$$

where  $L_n$  and  $L_p$  are the electron and hole diffusion length respectively.

The Fill Factor (FF) in eqn. (6) characterizes the non-linear electrical behaviour, thus determines the quality of the solar cell.

$$FF = \frac{V_{mp} \times I_{mp}}{V_{oc} \times I_{sc}} \dots\dots\dots (6)$$

where  $V_{mp}$  is the maximum voltage and  $I_{mp}$  is the maximum current.

The maximum power output from the solar cell can be written as eqn. (7):

$$P_{max} = (I_{sc} \times V_{oc} \times FF) \dots\dots\dots (7)$$

The power conversion efficiency can be expressed as in eqn. (8):

$$\eta = \frac{I_{sc} \times V_{oc} \times FF}{P_{input}} \dots\dots\dots (8)$$

### 3. Types of Solar Cells

Basically, here we will discuss only the following three types of solar cells: Mono or single crystalline (sc-Si), Multi or poly crystalline (mc-Si), and thin film solar cells (TFSC). Crystalline silicon is the most common type of solar cell among all those that we have. The reason behind it is that silicon is abundant and non-toxic; which is made of Sn sand. But, its major disadvantage is that the absorption of light by silicon is relatively weak, which in turn necessitates having a high thickness of the silicon layer in order to absorb the light efficiently and appropriately. Also, silicon is brittle material, which limits the lower boundary on its thickness. Along with that, the doping of silicon must be done in a clean environment to control the impurities if any. Because of this thickness limitation only, the material cost and thus the construction cost of silicon solar cells goes high. However, due to its inherent quality of lower defect density at the junctions, it has the highest energy conversion efficiency till date.

The sc-Si and mc-Si solar cells are very similar in their performance. The basic difference is that mc-Si based solar cells have slightly lower efficiency in compared to sc-Si based devices due to the difference in the defect structures, which are developed during the directional solidification or ingot casting in mc-Si while the crystal growth process was going on. It also leads to premature recombination of electrons and holes in mc-Si [22]. Along with that, sc-Si solar cells are more efficient in warm weather. So, as the temperature goes up its solar electricity output does not degrade severely as in mc-Si solar cells (in practice, the difference is very small) [7]. Hence, sc-Si is less expensive than mc-Si. Also, there is a provision that if we want to eliminate the waste during wafer slicing, continuous ribbon growth technologies such as Edge Film-fed Growth (EFG) and a process called String Ribbon could be adopted[22].

TFSC is a second-generation solar cell whose basic advantages are as follows: it is flexible; it involves a low-cost economy in terms of raw materials [21]. It has less weight per unit of power [7]. It shows good performance under low light conditions like during partial shading or in extreme heat, its mass production capability with varied sophisticated deposition techniques (like-homo, hetero and Schottky). It shows high light absorption capacity due to its extremely small thickness with small diffusion length, and its high recombination velocity makes it the cheapest type of solar cell in comparison to sc-Si and mc-Si solar cells (1st generation) solar cells. But, a little amount of disadvantage is that it is somewhat less efficient, requires more space for orientation [10] and has fast degradation which implies shorter life span in comparison to (sc-Si and mc-Si). TFSCs

are basically made of materials such as amorphous silicon (a-Si), cadmium telluride (CdTe) and cadmium indium gallium selenide (CIGS) or cadmium indium selenide (CIS). It is comprised of several layers consisting of different elements like the absorbing layer, an oxide layer, which is transparent and conducting (TCO) or called as transparent conducting oxide, a window layer, and rear metal contact layer [22]. The properties of all of these layers and its interfaces are the optimum factors that affect the actual efficiency of the cell.

Again, we have organic and inorganic thin film solar cells. Organic solar cells are several times thinner than inorganic solar cells, thus have high absorption capacity; so it has a slightly higher efficiency. Along with that, organic solar cells have a higher affinity for chemical modification or one can say that via chemical synthesis techniques, several arrangements or modifications could be done at molecular level adjustments (better than atomic level arrangements) [4]. But, if we see the energy required to dissociate the excited states or excitons (formed by the absorption of photons), it is approx 0.5 eV for organic, whereas few milli eV for inorganic. Some examples of organic solar cells are fullerene, polypyrrole, polyaniline, etc. Some examples of inorganic solar cells are CdS, CIGS, cadmium selenide (CdSe), etc. Along with that, by combining organic matter and inorganic matter, one more types of solar cell called biohybrid solar cells had been developed by the researchers [12,13]. Hence, the organic photovoltaic devices have the advantage of low weight, good flexibility, semitransparent, easily gets integrated into other products, less manufacturing cost, shorter period of energy payback, etc. [3,16].

The voltage rating ( $V_{mp} / V_{oc}$ ) of the crystalline is around 80% to 85% whereas for thin film is around 72% to 78% [10]. Along with that, the temperature coefficient and fill factor value of the thin film is lower than a crystalline silicon [10]. As the absorbing layer gets thinner; its light-absorbing capacity goes on enhancing. Hence, TFSC is a journey to attain the highest efficiency level that could be achieved from light. We have two types of configurations for the thin film: the superstrate and the substrate as shown in Figure 3. The main difference between these is that the substrate, which provides a layer of support to the thin film cell. Superstrate type has a transparent glass substrate, e.g. CdTe. Substrate type has a non-transparent substrate (metal or metallic coating on a glass/plastic), e.g. CIGS/CIS. Substrate type is cheaper comparatively [22]. But, the major disadvantage of the CdTe and CIGS is that cadmium is toxic which causes environmental problems; as well as Indium and Gallium are very rare metals that are available.

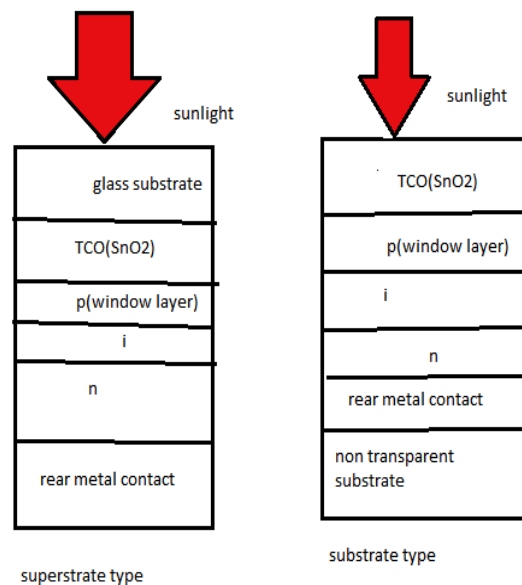
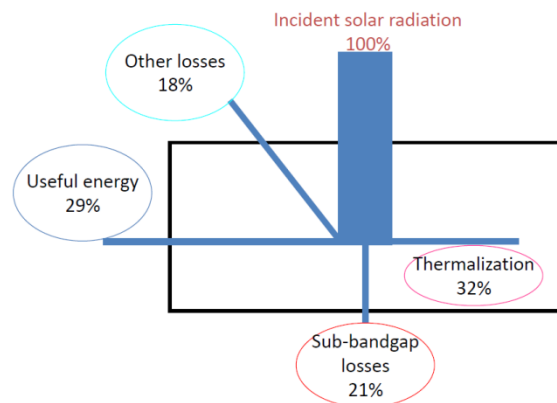


Figure 3: Types of configurations [22]

#### 4. Losses of Incident Light Over the PV Cell

The whole portion of the incident light over the PV cell is not converted into electrical energy as shown in Figure 4. A major amount of it gets lost due to the following reasons. Since, every differently composed PV material has a specific range of spectral bandwidth that it is suited for, hence if the bandwidth of light incident does not match with the particular cell requirement, then the PV cell does not absorb that light; instead, that light creates only heat on the surface of the cell, which is not purpose. Recombination, resistive heating, electrical resistance losses or the electrical interconnects, shadowing, module inefficiency, optical reasons like scattering and reflection (highest loss) at the surface of the solar cell are also the factors that contribute to the system loss. By creating cohesive (well bonded) surfaces and interfaces within the solar cells, the losses during manufacturing could be prevented [22]. With a motto to improve the light trapping or light absorption, manufacturers try to modify the design of a solar cell in such a way that whatever the light enters its path length, should be there as long as possible for better absorption of light by the cell [5]. Actually, here in order to improve the absorption of light, the top contact coverage layer surface of the solar cell has to be minimized in order to reduce the amount of area that blocks light from reaching the cell [20]. Practically, only about 25% to 29% of the incident light energy can be converted into electrical energy.



**Figure 4:** Losses in a solar cell [9]

## 5. Antireflection Coatings

The prime objective of the antireflection technique is to trap more light in compared to that the cell could originally do. A coating of anti-reflecting material is provided on the very top layer of the solar cell in order to reduce the optical losses (normally reflection) when the light is incident on the surface of the cell. The coating layer may be mono or double depending on the user requirement. If the amount of light, which is reflected back could be reduced to an optimum level or reducing the surface recombination, then only the absorbing level as well the conductivity level of the cell could be increased and in turn, the efficiency level could be enhanced to a certain extent. Monolayer coating, generally of  $\text{SiN}_x$  or  $\text{SiO}_2$ , has the lowest reflectivity but it shows its good result only within a certain small bandwidth. And, the double layer coating is formed by combining  $\text{SiN}_x$  and  $\text{SiO}_2$ . Double layer coating is created by oxidizing the Si surface first at high temperature and then a Plasma-Enhanced Chemical Vapor Deposition (PECVD) coating of  $\text{SiN}_x$  is applied to it. A better quality of  $\text{SiN}_x$  is obtained if it is deposited by employing high-frequency PECVD. (TCO) also performs as an anti-reflection coating or as a conductive electrode, which creates voltage depending on the photoelectric effect. It has a wide bandgap and it is transparent for the visible light [22], e.g. indium doped tin oxide, Aluminium doped zinc oxide, etc. Along with that, at the bottom, reflecting coating layer should be used to a certain extent such that there would be a total internal reflection of the absorbed light and hence more absorption and thus higher conductivity [22].

### 5.1 Types of Antireflection Coating Methods

(a) An antireflection technology, where the black silicon coating (black colour absorbs more light even at lower angles with very less reflectivity [11]) is provided on the top the solar cell is catalysed in order to create a layer where the

refractive index gradually changes when the light is incident on it. Here the motto behind is to create a layer of nanostructures whose light absorbing wavelength limit is less than the wavelength of incident light. Along with that grading is done across the thickness of the silicon layer. This small modification in the refractive index of the coating layer enables the light to penetrate further into the cell instead of being reflected away; thus the light absorption is enhanced [23].

(b) Pyramidal texturing (in Figure 6) is one more antireflection technology, which etches away the material used on the top of the solar cell in order to create very small pyramid-like structures. Now, when light (photon) incident on these pyramidal structures, it either gets absorbed or reflected onto another pyramid, creating another opportunity for the photon to get absorbed as much as possible. By this way, these pyramids effectively enhance the chance for the photon to get absorbed. Generally, TMAH (Tetra Methyl Ammonium Hydroxide) is used with the silicon surface with the motto to create reliable pyramidal structures. Now a better idea is that if both the black silicon and pyramidal texturing method is combined as shown in Figure 5, then the light absorption could be doubly enhanced. It decreases the amount of blue light recombination as well as it creates an even better antireflection possibility. However, passivation and difficulty in large-scale applications are its two weaknesses [21].

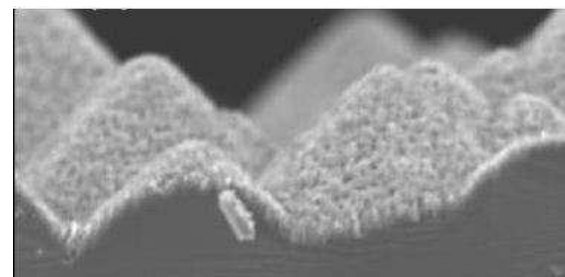


**Figure 5:** Cross section of black silicon with pyramid architecture [22]

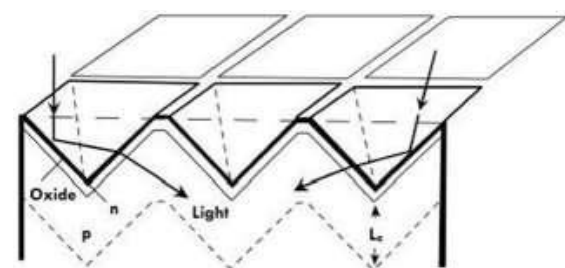


**Figure 6:** Inverted pyramid structure [22]

(c) One more method of antireflection technology that appears almost similar to the pyramidal texturing methods is moth-eye texturing, which

employs the idea of formation of pillars with narrowed structural orientation as appears in moth eyes, as shown in Figure 7. But, this moth eye creation process is an expensive step, because pillar-like structures with higher ratios are difficult to create and align [22].



Figure 7: Moth texture [23]

(d) One more method is to form a bump and sponge-like nanostructures by growing a thin layer of (SiO<sub>2</sub>) on triacetate polymers in as shown in Figure 8. Here the (SiO<sub>2</sub>) provides dual protection; it enhances performance as well as provides a protective layer to the nanostructures that are developed [22].

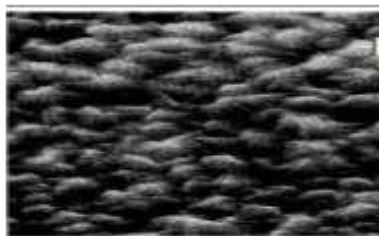


Figure 8: Bump structure [22]

(e) We have one more option for the antireflection method and that is to use a large grain size (SnO<sub>2</sub>) thin film over the top layer as shown in Figure 9. Due to its rough surface texture, it improves the light trapping by the solar cell [22].

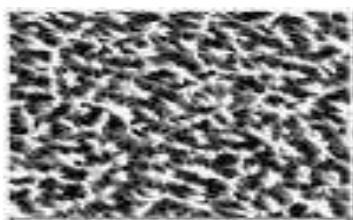


Figure 9: Thin film of SnO<sub>2</sub> on top layer [22]

## 6. Plasmonics

Generally, errors arise when the thin film solar cells trap light and plasmonics acts as a solution to the said problem as shown in Figure 10. Plasmonics are actually defined as the resonant oscillations of free or conducting electrons collectively between a metal and a dielectric or positive and a negative permittivity materials, which is stimulated by incident light as a source

thus resulting into a resonant frequency [15]. It is also broadly described as the interaction of conducting electrons (charges with the EM waves). When the wavelength of incident light converges with the wavelength of the oscillatory wave, i.e. Plasmon, then it leads to higher absorption of photons. These plasmons act like dipoles. Here, the wave is only due to the oscillation of nano particles that happens due to the interaction between the charges. Size, shape, and dielectric properties of the medium are the factors, on which the formation of surface plasmon wave depends. An ideal plasmon wave does not have nodes in the semiconductor. Metals formed of noble gas compounds are best applicable for the nano particles when used for the PV purposes because it shows resonance in the infrared and visible frequencies [22].

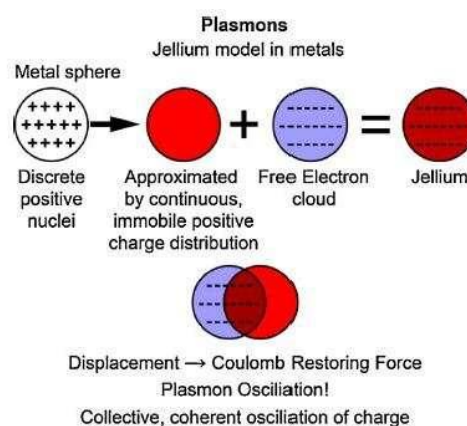


Figure 10: Plasmon [22]

## 7. Negative Index Metamaterials (NIM)

NIM is a method of improving light absorption and reducing the light reflecting back. It is an artificially man made material whose observed properties are not seen in nature. It refracts the incident light on the same side of the normal to the surface (opposing the standard rule of light refraction) as shown in Figure 11. A small change in the geometry of the NIM structures causes the refractive index to become positive; it implies that structures exhibiting NIM property are extremely sensitive to its geometry. Actually, NIMs are the improved version of fishnet structure (as shown in Figure 12), which is a combination of a cross and a circle employed for linear polarizations arbitrarily. Within the improved structure, the current density is very high, thus it leads to a high magnetic resonance [22].

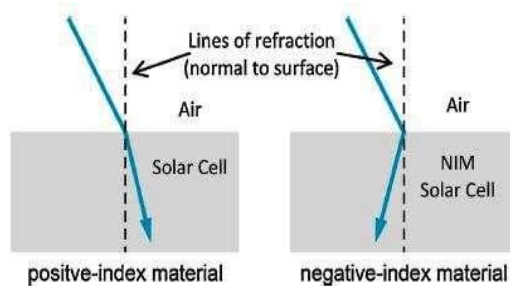


Figure 11: NIM refraction property [22]

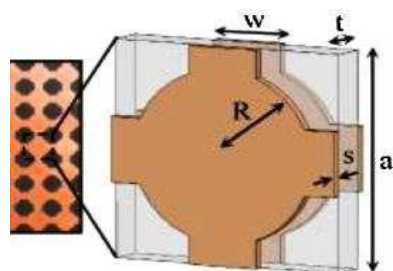


Figure 12: NIM fishnet structure [22]

## 8. Solar Multijunctions

The construction of practically powered PV modules becomes possible by changing the material from amorphous silicon (a-Si) to amorphous silicon hydrogenated (a-Si:H), because a-Si:H is well suited for doping and alloying with other materials and fabrication of junction devices. But, a single junction (a-Si:H) solar cell faces the problem of degradation of the material when induced by the light for a long time. Thus, it leads to the reduction in the energy conversion efficiency in the very initial stage of operation of the solar cell and following to it that solar cell then stabilizes at a lower efficiency (approximately 30% less than the initial value). So, one possible solution could be the use of a thin intrinsic layer in order to generate a high internal electric field and lessen the sensitivity to the distortions appeared. But, this thin intrinsic layer, further results in the reduction of absorption of light or energy by the solar cell. However, this amount of reduction in efficiency due to a low amount of light absorption could be compensated to some extent by the multiple p-i-n structures, which is composed of several amorphous silicon layered structures as shown in Figure 13. Thus, a heterodyne junction is created by using multiple p-i or i-n junctions. The mc-Si has a higher electron mobility as well as a high light absorption coefficient due to the presence of silicon crystallites. Multijunctions are best suited for concentrator solar plants [22].

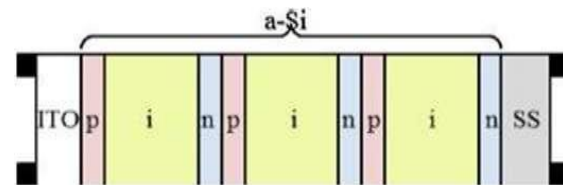


Figure 13: Multilayered a-Si solar cell [22]

Now, in order to connect the multijunctions, wafer bonding and layer transfer processes are used. In wafer bonding [22] (interface made is very strong), the two materials that are required to be bonded to be atomically flat. After that, they are pressed together and heated up, and due to their planarity property atoms are allowed to diffuse between the materials; as a result of which current easily passes through it thus enhances the efficiency. And, the other method is the layer transfer processes [22], in which the crystalline films are grown on an expensive substrate (reusable) and then moved to create the multijunction.

## 9. Environmental Impact on Solar Cell

### (i) Effect of dust on the PV cell's performance:

The minute solid particles whose size is less than 500 nm in diameter are regarded as dust. Once the dust is deposited on the cell, it attracts more dust to be deposited; so better is that the already deposited dust has to be removed as fast as possible. The dust settlement on solar module depends on the tilted angle and the finishing of the surface of the module, as well as humidity and wind speed prevailing in the environment at that moment. If the modules are tilted at a large angle, then a lesser amount of dust is deposited; and thus the drop in transmittance reduces. Fine dust particles are more dangerous than the coarser dust particles. High wind speed leads to high deposition of dust on the module; thus leads to the deterioration of the module. Along with that higher humidity level enhances the dew formation on the top of the module, and if in that period wind flows with fine dust; then the highest amount of dust will get deposited; hence the poor output of the module [19].

### (ii) Effect of wind velocity on PV cell performance:

With the increase in the air velocity, the temperature of the solar cell drops, which implies a better PV cell efficiency [19]. However, as mentioned earlier, high wind speed leads to dust deposition on the module. There is another side to it called shading, which happens due to the scattering of dust as well as nearby particles due to

high wind speed; thus, leads to poor performance of the solar system as depicted by the in eqn. (9).

$$\text{Performance Ratio} = \frac{P_{mean} \times P_{max}}{G} \dots\dots\dots (9)$$

where,  $P_{mean}$  = mean power output (W);  
 $P_{max}$  = maximum power output (W)

**(iii) Effect of Humidity on PV Cell Performance**

As mentioned earlier, high humidity leads to dust deposition on the module. Along with that, there are two directions, which need to be monitored [19]. The first side is that the effect of water vapour particles on the irradiance level of sunlight and the second way is the humidity ingress in the solar cell enclosure. Light after hitting the water droplets may be refracted, reflected or diffracted. There is a non-linear effect of humidity on the irradiance of sunlight as shown in Figure 14. Moreover, irradiance creates little variations in a non-linear manner and creates large variations linearly as shown in Figure 15. This non-linearity is due to the non-uniform distribution and wide range of the size of water vapour particle. Also, the scattered angle is inversely proportional to the size of water vapour particles.

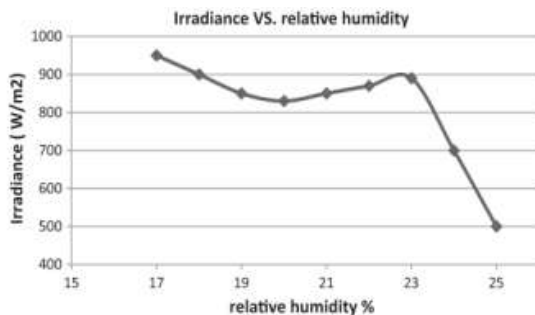


**Figure 14:** Solar irradiance v/s Relative Humidity [19]

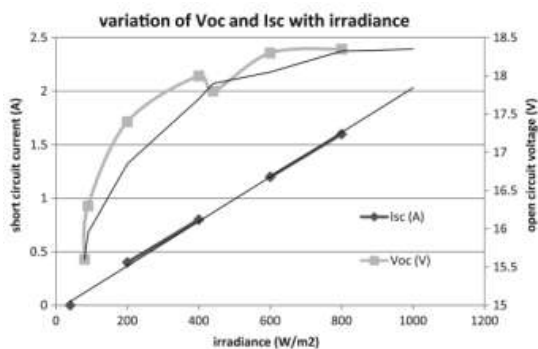


**Figure 15:**  $V_{oc}$  and  $I_{sc}$  v/s Solar irradiance [19]

**10. Reliability of PV Cell**

The necessary parameters that are required in order to determine the break-even characteristics of PV modules are reliability and longevity. All those etching steps that are adopted in order to remove the cracks or defects that are formed during the wafering process while manufacturing if fails in its performance, then the module shows problems in its operation. Here we can not discard the situation of performance degradation by the solar cell in the interfaces completely; it will be present even in a very small scale also; because always a heat is generated on the cell when the photon is incident on it or we can say heat is a by-product of photon energy conversion. In order to obtain a cell with good reliability conditions; the interfaces that we have in the solar cells must be robust against the thermal cycling. Cracks may also be seen during the mechanical movement of the solar cell like when the cell was being installed or maybe during transportation. Sometimes, cracks may also appear due to the moisture seepage caused by rain; thus, dew gets into any slight cracks hence percolate into the cells ultimately leads to the non-uniformity of the interfaces; in turn the performance of the solar cell deteriorates, e.g. light absorption capacity gets reduced, moisture absorption increases hence critically damages the cell. A large amount of heat and UV radiation is developed on those multijunctions that are applied in concentrator solar systems, which in turn, the lifetime of the cell diminishes. So, as a solution to achieve the reliability conditions or to avoid the cell failure, the material used for the construction must have the properties like- robustness, durability, heat resistant, water resistant, flexibility [22].

**11. Cost**

The cost required in order to construct a solar cell governs by both the reliability and efficiency of the solar cell. The cost incurred is subdivided into Short-term cost and Long-term cost [22]. Short-term cost includes the cost of buying the raw materials cost, installation as well as transportation, then manufacturing cost, reliability testing cost. Long-term cost is basically based on life expectancy of the solar cell which involves the cost of maintenance like replacing the cells after prolonged use. Ultimately, our main aim is to determine the solar cell with the best design and least cost as much as possible without sacrificing efficiency and reliability. But, there is a general logic that the cells with high efficiency are more costly. Likewise, cadmium is too toxic; tellurium and indium are so rarely found that it cannot provide a strong support to the total energy production. Hence, a trade-off will always be there in order to maintain balance between efficiency,

reliability and cost. Energy payback is a very complicated metric to calculate, because of the large variance in data obtained. Payback period varies from one cell to the other depending on factors like- type of raw material used, installation location, reliability, and manufacturing processes. The standard lifetime for a solar cell is generally 30 years (bulk production of solar cell always has a lesser efficiency than a cell that is developed in a lab, because when constructed in bulk it generates heat which further reduces the efficiency of the solar cell). Applications of solar cells include power plants, homes, commercial uses, ventilation systems, remote applications, solar cars, solar lightings, etc. [11].

## 12. Market Share and Efficiency

If we look on market share with present efficiency levels (as obtained from the website of National Renewable Energy Laboratory ([www.nrel.com](http://www.nrel.com))). In 2013, TFSC accounted for about 9%. In 2015, TFSC accounted for about 9(+7)%. Rest of the per cent is occupied by crystalline silicon (sc-Si and mc-Si). PCE, i.e. power conversion efficiencies of different types are shown in Figure 16. Some of the current solar cell manufacturing market leaders are mentioned here [14].

For crystalline silicon: Sharp, Kyocera, Suntech, etc.

For a-Si: Sharp, United Solar, Fuji Electric, etc.

For CdTe: First Solar, Antec Solar

For CIGS: Day Star, Shell Solar, Wurth Solar, etc.

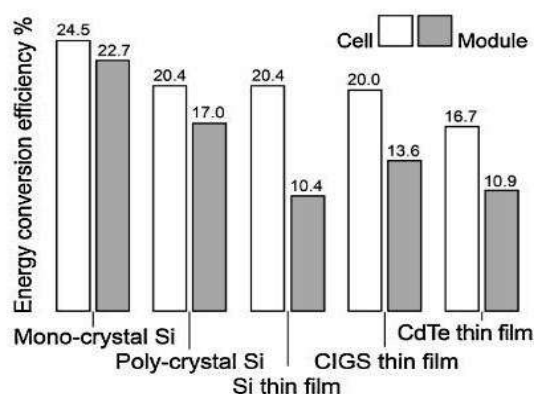


**Figure 16:** Power Conversion Efficiency (PCE) [22]

## 13. Conclusion

In this review, the basics on p-n junction and further formation of a solar cell, along with the necessary characteristic equations have been discussed. The types of solar cells have been discussed in detail, with more concentration of work on thin-film solar and its different contributions due to its several advantages.

However, every system has a loss associated with it. Few more methods were discussed like antireflection coating, multijunction, negative index metamaterials, plasmonics in order to construct a cell in such a way that its light absorption capacity gets enhanced in turn efficiency. Also, we came to know how the solar cell or a module responds towards the environmental impacts, e.g. dust, wind velocity and humidity. A review of the analysis has also been done in order to determine the reliability or longevity as well as the cost incurred. And finally, we have mentioned about the market share and the efficiency chart as obtained from the National Renewable Energy Laboratory.

The combination of the following factors determines the performance of solar cells: Radiation at the site, Losses in PV systems, Amount of light absorbed and reflected, Temperature and climatic conditions, Design parameters of the plant, Inverter efficiency, Module Degradation due to ageing, etc. [23].

Efficiency, in decreasing order, can be arranged as: sc-Si > mc-Si > thin film

The cost in decreasing order can be arranged as: sc-Si > mc-Si > thin film.

Additionally, thin film solar cells have an approximate lifetime of 20 years and Crystalline solar cells have an approximate lifetime of 25-30 years lifetime. In, India, the Government is carrying out a mission under the name of Jawaharlal Nehru National Solar Mission (JNNSM). Its objective is to create a policy framework for the creation of 20,000 MW from solar source by 2022 [23].

## References

- [1] K. Fotis, *Modeling and simulation of a Dual-Junction CIGS solar cell using Silvaco ATLAS*, Master's Thesis, Naval Postgraduate School, Monterey, CA, Dec. 2012. Retrieved from <https://apps.dtic.mil/dtic/tr/fulltext/u2/a574282.pdf>
- [2] S. Sharma, K. K. Jain and A. Sharma, "Solar Cells: In Research and Applications - A Review", *Materials Sciences and Applications*, Vol. 6, Issue 12, 2015, 1145-1155. Doi: <http://dx.doi.org/10.4236/msa.2015.612113>
- [3] A. M. Bagher, "Comparison of organic solar cells and inorganic solar cells", *International Journal of Renewable and Sustainable*

- Energy, Vol. 3, Issue 3, May 2014, pp.53-58. Retrieved from <https://pdfs.semanticscholar.org/6b7e/974a3954093be6456189b879d325a3651ffa.pdf>
- [4] S. L. Arora, "Chapter 14 - Semiconductor devices and digital circuits", in *New Simplified Physics: A Reference Book for Class 12*, Volume II, Dhanpat Rai & Co. 2016 Edition
- [5] J. Gjessing, *Photonic crystals for light trapping in solar cells*, Ph.D Thesis, University of Oslo, Norway, Oct. 2011. Retrieved from <https://www.osti.gov/etdeweb/servlets/purl/21573466>
- [6] "Pros and Cons of Monocrystalline vs Polycrystalline solar panels", [www.solarreviews.com](http://www.solarreviews.com) [Online]. Available: <https://www.solarreviews.com/blog/pros-and-cons-of-monocrystalline-vs-polycrystalline-solar-panels> (Accessed: 11 Feb. 2017)
- [7] Y. Chu and P. Meisen, "Review and comparison of different solar energy technologies", Technical Report, Global Energy Network Institute (GENI), San Diego, CA, Aug. 2011. Retrieved from <https://www.geni.org/globalenergy/research/review-and-comparison-of-solar-technologies/Review-and-Comparison-of-Different-Solar-Technologies.pdf>
- [8] S. O. Kasap, *Principles of Electronic Materials and Devices*, 3<sup>rd</sup> Edition, McGraw-Hill, NY, 2006.
- [9] K. L. Chopra, "Thin Film Solar Cells: A Status Review, Thin Film Laboratory, IIT Delhi & Microscience Laboratory, IIT Kharagpur. [Online]. Available: <http://www2.kfupm.edu.sa/cent/img/kfupm-tfsc-dec20.pdf>
- [10] L. Bas. "Thin Film vs. Crystalline Silicon PV Modules", *CivicSolar, Inc.*, 2010. [Online]. Available: <https://www.civicsolar.com/support/installer/articles/thin-film-vs-crystalline-silicon-pv-modules> (Accessed: 11 Jan. 2017)
- [11] A. M. Bagher, M. M. A.Vahid and M. Mohsen, "Types of Solar Cells and Application", *American Journal of Optics and Photonics*, Vol. 3, Issue 5, 2015, pp. 94-113. Retrieved from [http://barghnews.com/files/fa/news/1397/10/27/72825\\_110.pdf](http://barghnews.com/files/fa/news/1397/10/27/72825_110.pdf)
- [12] P. N. Ciesielski, F. M. Hijazi, A. M. Scott, C. J. Faulkner, L. Beard, K. Emmett, S. J. Rosenthal, D. Cliffler and G. K. Jennings, "Photosystem I - Based biohybrid photoelectrochemical cells", *Bioresource Technology*, Vol. 101, Issue 9, 2010, pp. 3047-3053. Doi: <https://doi.org/10.1016/j.biortech.2009.12.045>
- [13] O. Yehezkeli, R. Tel-Vered, J. Wasserman, A. Trifonov, D. Michaeli, R. Nechushtai and I. Willner, "Integrated photosystem II-based photo-bioelectrochemical cells", *Nature communications*, Vol. 3, Article No. 742, March 2012. Doi: <https://doi.org/10.1038/ncomms1741>
- [14] K. Molter, "Lecture 3: Types of Solar Cells (experiment)- 3 generations", Class lecture material, *Clemson Summer School, fh trier, Trier University of Applied Sciences*, Retrieved from <http://www.cie.unam.mx/lifycs/ITaller2011/PV-Tutorial2011/Lecture3-AH.pdf>
- [15] "Surface plasmon resonance", *Wikipedia*. [Online]. Available: [https://en.wikipedia.org/wiki/Surface\\_plasmon\\_resonance](https://en.wikipedia.org/wiki/Surface_plasmon_resonance) (Accessed: 12 Jan. 2017)
- [16] M. C. Scharber and N. S. Sariciftci, "Efficiency of bulk-heterojunction organic solar cells", *Progress in Polymer Science*, Vol. 38, Issue 12, 2013, pp.1929-1940. Doi: <https://doi.org/10.1016/j.progpolymsci.2013.05.001>
- [17] A collection of resources for the photovoltaic educator, [Online]. Available: [www.pveducation.org](http://www.pveducation.org) (Accessed: 12 Jan. 2017)
- [18] Website of National Renewable Energy Laboratory (NREL). [Online]. Available: [www.nrel.com](http://www.nrel.com) (Accessed: 10 Dec. 2010)
- [19] S. Mekhilef, R. Saidur and M. Kamalisarvestani, "Effect of dust, humidity and air velocity on efficiency of photovoltaic cells", *Renewable and Sustainable Energy Reviews*, Vol. 16, Issue 5, 2012, pp. 2920-2925.
- [20] "Thin-film solar cell", *Wikipedia*. [Online]. Available:

[https://en.wikipedia.org/wiki/Thin-film\\_solar\\_cell](https://en.wikipedia.org/wiki/Thin-film_solar_cell) (Accessed: 12 Jan. 2017)

- [21] M. A. Green, "The Future of Thin Film Solar Cells", *Proc. of ISES World Congress 2007 (Vol. I-Vol. V)*, Springer, Berlin, Heidelberg, 2008, pp. 96-101. Doi: [https://doi.org/10.1007/978-3-540-75997-3\\_14](https://doi.org/10.1007/978-3-540-75997-3_14)
  
- [22] A. Chandra, G. Anderson, S. Melkote, W. Gao, H. Haitjema and K. Wegener, "Role of surfaces and interfaces in solar cell manufacturing", *CIRP Annals - Manufacturing Technology*, Vol. 63, Issue 2, 2014, pp. 797-819. Retrieved from [https://www.icvr.ethz.ch/ConfiguratorJM/publications/Role\\_of\\_su\\_142199966557759/2014\\_63\\_2\\_0797\\_S\\_final.pdf](https://www.icvr.ethz.ch/ConfiguratorJM/publications/Role_of_su_142199966557759/2014_63_2_0797_S_final.pdf)
  
- [23] B. D. Sharma, "Performance of Solar Power Plants in India", Technical Report, *Central Electricity Regulatory Commission*, New Delhi, India, Feb. 2011. Retrieved from <http://www.cercind.gov.in/2011/Whats-New/PERFORMANCE%20OF%20SOLAR%20POWER%20PLANTS.pdf>

# A Review on Wireless Power Transfer

Parveen Kaur

Department of Electrical and Electronics Engineering, School of Technology, Assam Don Bosco University,  
 Airport Road, Azara, Guwahati -781017, Assam, INDIA.  
 parveenkaur1994@gmail.com

**Abstract:** This paper is a review of the various designs put forward by various people regarding the Wireless Power Transfer (WPT). Here the designs have been discussed, along with the purpose that the design can be used for, the efficiency of the power produced and also the ways to improve the efficiency of the design. The values of various parameters and diagrams used are based on the experimental results of various researchers. Finally, a suitable conclusion has been drawn regarding the best design, which can be used for WPT taking into consideration the various associated factors that have been discussed here.

**Keywords:** Wireless Power T (WPT), Inductive Coupling-coil Optimization, Class E<sup>2</sup> DC-DC converter, Maximum DC-DC efficiency, Particle Swarm Optimization, Class E rectifier, Resonant wireless power transfer, Power Conversion Efficiency (PCE).

## 1. Introduction

Today’s world is governed by various new invention and technological advancements. Life is now quite easier; everything is just a click away. We have wireless Internet, phones, laptops, earphones and so on; wireless pieces of stuff are the new trend of the generation. Still, at some point of the day, we are still tied to the codes as all those devices have batteries, which need to be recharged and for that, we have to plug in the devices. So why not design a Wireless Power Transfer (WPT) device. Wireless Power Transfer (WPT) will be of great help not only for our day-to-day lives but also in the medical field. In our day-to-day lives, we will not have to limit ourselves to the use of a cord. In medical, it will be a convenient way to supply power to small implanted devices such as pacemakers and many more. Now we know Wireless Power Transfer (WPT) can be of great use, but with that, a series of questions arise like: Is WPT even possible? If yes, then how to construct such a device that will provide WPT? What will be its efficiency? ...and many more.

There are numerous researches going on with WPT and various designs are being put forward having different efficiency levels depending upon the purpose they are going to serve. In this paper, some of the designs will be reviewed and respective uses and efficiency will be discussed.

## 2. Wireless Power Transfer Designs

Wireless power transfer (WPT) is the transmission of electrical energy from a power

source to an electrical load, such as an electrical power grid or a consuming device, without the use of discrete human-made conductors. The various designs discussed in this paper are as follows:

(i) Researchers Takumi Noda *et al.* in their research titled “Design Procedure for Wireless Power Transfer System with Inductive Coupling Coil Optimization Using PSO” [2], presented a design procedure for the WPT system based on the class-E<sup>2</sup> dc-dc converter, taking into account the inductive coupling-coil optimization.

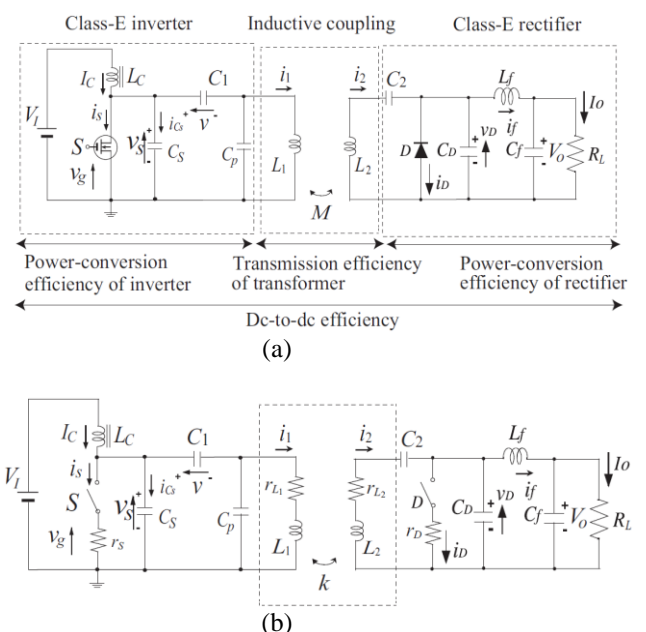


Fig. 1: Class-E<sup>2</sup> WPT System: (a) System Overview (b) Equivalent circuit model for dc-to-dc efficiency calculation

Here dc-to-dc efficiency, defined as the ratio of the output power to the input power namely the dc-to-dc efficiency, includes the transmission efficiency of the coupling coils, and power conversion efficiency of the power converter. A class-E switching circuit is used because the class-E inverter and the class-E rectifier satisfy zero-voltage switching and the Zero-Derivative Switching (ZVS/ZDS) condition and the WPT can achieve a high dc-to-dc efficiency at high frequencies because of the zero switching loss in the power converter.

By using the analytic expression, the authors mentioned that it was possible to express the coupling part as a transformer model with low coupling coefficient, which is a function of the physical parameter such as a coil diameter, coil height and so on. The Particle Swarm Optimization (PSO) is used for reducing the computational complexity. Moreover, the laboratory measurements agreed with analytical design predictions, which show the validity and usefulness of the proposed design procedure. The dc-to-dc efficiency is a cost function with is maximized by using PSO algorithm. They used an air core coil as the core materials are limited by the operating frequencies and it is difficult to obtain a desired shape of the core.

The main challenge faced while constructing this type of WPT is the necessity to obtain proper components value accurately, which is a design problem of class-E circuit design. Through experimental verification, it is seen that the measured dc-to-dc efficiency at 3.0 cm coil distance was 81.1% at 12.8 W output and 1MHz operational frequency. The efficiency can further be increased by using class-EF or class-E/F<sup>3</sup> inverters as they produce 43% and 24% more power than that of a class-E inverter respectively.

(ii) Authors Pham Tuan Anh and M. Chen in their research titled “Design and Optimization of High Efficiency Resonant Wireless Power Transfer System” [3], have used the concept of magnetic resonant coupling as it is the most promising candidate for the midrange transfer of power because of its long range and compact dimension. And also the concept of high-efficiency Resonant Wireless Power Transfer (RWPT) system as it discusses the optimal parameters for maintaining high power transfer efficiency with respect to distance and load variation.

The circuit representations are shown below in Figures 2(a), 2(b) and 2(c).

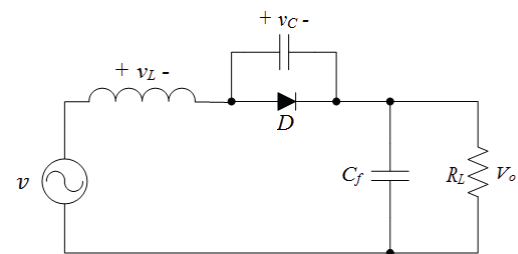


Fig. 2(a): Class E resonant voltage-driven low dv/dt rectifier circuit.

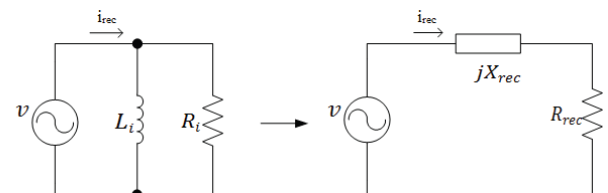


Fig. 2(b): Circuit model for the input impedance of the class E resonant voltage-driven low dv/dt rectifier

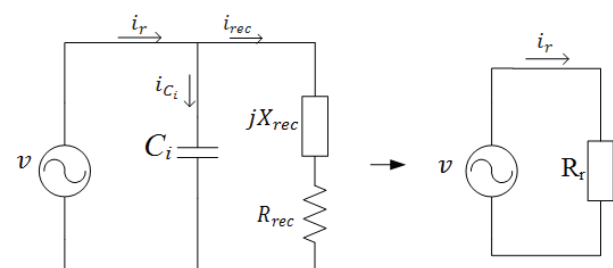


Fig. 2(c): Rectifier impedance with a parallel capacitor

The proposed system consists of a class-E amplifier with a 6.78 MHz resonant frequency coupling coils and a class E rectifier. It can be used in a variety of application such as biomedical devices, automotive systems, industrial manufacturing and some consumer electronics while operating at high levels (such as 6.78 MHz and 13.56 MHz), which can enable charging multiple devices simultaneously.

The output voltage  $V_0$  produced in this case is DC and ripple free. To minimize the voltage and current stress on the diode, as shown in Fig. 2(a), a class-E rectifier is usually designed to have a 50% duty cycle for the rectifying diode. In addition, to improve the power factor of the rectifier a capacitor is introduced in parallel with  $Z_i$  as seen in Fig. 2(c). The power factor of the combined load capacitor impedance is unity.

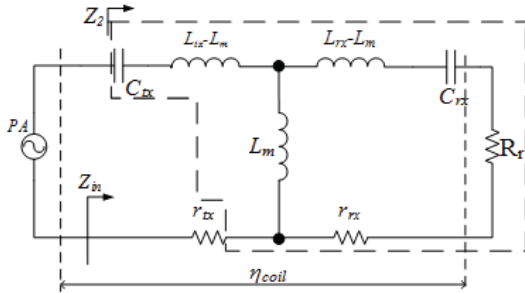


Fig. 2(d): Circuit model of coupling coils

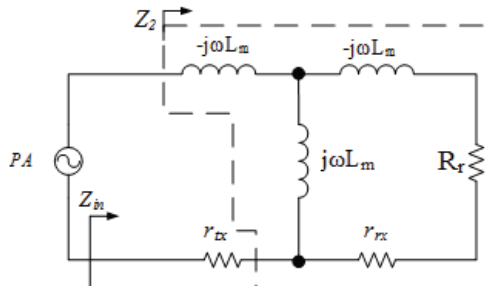


Fig. 2(e): Circuit model of coupling coils at resonant frequency

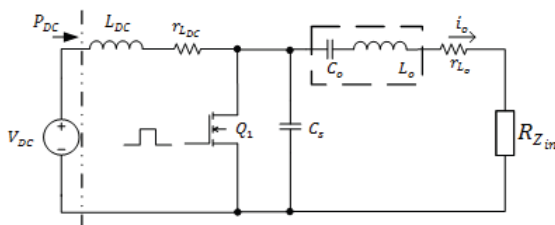


Fig. 2(f): Circuit model of the class E power amplifier

The Figures 2(d), 2(e), and 2(f) represent the circuit model of coupling coils, the circuit model of coupling coils at the resonant frequency and the circuit model of the class-E power amplifier respectively.

After simulating the RWPT system using MATLAB Simulink, a resonant efficiency of 93% was achieved when the mutual inductance coefficient of  $k = 0.2$  was taken at a resonant frequency of 6.78 MHz.

(iii) The authors Hiroto Sakaki *et al.* in their research titled “A Novel Wide Dynamic Design for Wireless Power Transfer System” [1], proposed a novel wide dynamic range rectifier for Microwave Wireless Power Transfer (MPT). The key component of MPT is a high-efficiency RECTENNA (Rectifier + Antenna). They proposed a new topology for a wide range dynamic rectifier without switches (i.e. no switching loss at all) that achieves high RF-DC power conversion efficiency. This idea is founded on two types of diode that have different threshold voltages. One is a low threshold voltage diode (HSMS-285: Avago Tech). The other is a high threshold voltage diode

(HSMS-286: Avago Tech). The circuit representation is shown below in Figures 3(a) and 3(b).

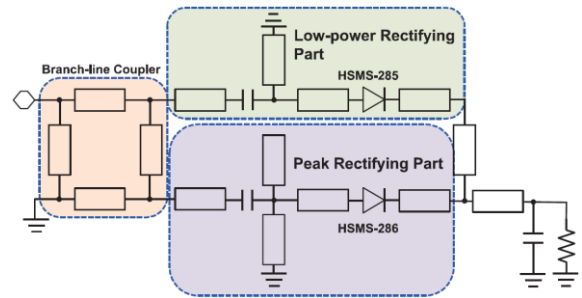


Fig. 3(a): Proposed wide dynamic range rectifier

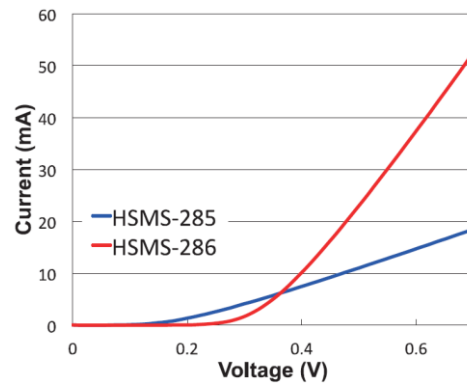


Fig. 3(b): Current-Voltage Characteristics of these diodes

The red line is for HSMS-285 and the blue line for HSMS-286. HSMS-285 deals in case of low input power; whereas HSMS-286 deals with high input power (HSMS-285 is also active at high input power). The proposed rectifier configuration at two different configurations can be better understood from Figures 3(c) and Fig. 3(d), which represent the operation at low-level input and at high-level input.

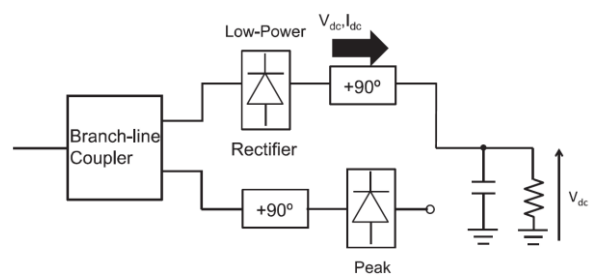
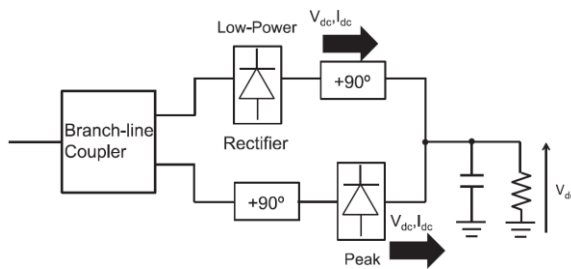


Fig. 3(c): Proposed Rectifier Configuration (Operation at low input levels)



**Fig. 3(d):** Proposed Rectifier Configuration (Operation at high input levels)

During the low input level, only low-power rectifying part is active whereas the peak rectifying part is inactive as the input power is not enough to turn on the peak rectifier. But, in case of high input level both the parts, namely low power rectifying part and peaking rectifying part are active. The F-DC power conversion efficiency is given by:

$$\eta = \frac{V_{in}^2}{P_{in} \cdot R_{out}} \times 100$$

where  $\eta$ ,  $P_{in}$ ,  $V_{in}$ ,  $R_{out}$  are Power Conversion Coefficient, RF Input Power, DC Output Power, and Optimum Load Resistance respectively. The dynamic range of power conversion efficiency in excess of 50% is 4 dB higher than those alternatives reported in the research [1], which validates the proposal. The net efficiency of this model is 89%.

### 3. Conclusion

Wireless Power Transfer (WPT) is the transmission of electrical energy from a power source to an electrical load, such as an electrical power grid or a consuming device, without the use of discrete human-made conductors. We have discussed three different designs for WPT having different efficiency levels when operated at their respective domains. Out of these three pieces of research reviewed here, the model proposed by P. T. Anh and M. Chen [3] can be considered the most efficient of all at its respective domain. Other than that; for more dynamic design, the design proposed by H. Sakaki *et al.* [1] can be used as it offers more flexibility regarding performance. For more details, one can refer to their respective analysis. Various other designs for WPT are also available, one can choose depending on its requirements.

### References

[1] H. Sakaki, F. Kuroiwa, M. Tsujii, M. Muraguchi, K. Nishikawa, K. Kawai, H. Okazaki and S. Narahashi, "A novel wide

dynamic range rectifier design for wireless Power Transfer system", *Proc. of 2014 Asia-Pacific Microwave Conference*, Sendai, Japan, 4-7 Nov. 2014, pp. 1208-1210. Retrieved from <https://ieeexplore.ieee.org/abstract/document/7067614>

[2] T. Noda, T. Nagashima, X. Wei, M. K. Kazimierczuk and H. Sekiya, "Design procedure for wireless power transfer system with inductive coupling-coil optimizations using PSO", *Proc. of 2016 IEEE International Symposium on Circuits and Systems (ISCAS)*, Montreal, QC, 22-25 May 2016, pp. 646-649. Doi: 10.1109/ISCAS.2016.7527323

[3] P. T. Anh and M. Chen, "Design and optimization of high-efficiency resonant wireless power transfer system", *Proc. of 2016 International Conference on System Science and Engineering (ICSSE)*, Puli, 7-9 July 2016, pp. 1-4. Doi: 10.1109/ICSSE.2016.7551636

[4] T. Noda, T. Nagashima and H. Sekiya, "A design of inductively coupled wireless power transfer system with coupling coil optimization", *Proc. of 2015 IEEE International Telecommunications Energy Conference (INTELEC)*, Osaka, 18-22 Oct. 2015, pp. 1-6. Doi: 10.1109/INTLEC.2015.7572277

[5] J. H. Holland, *Adaptation in Natural and Artificial Systems: An Introductory Analysis with Applications to Biology, Control, and Artificial Intelligence*, 2<sup>nd</sup> Edition, MIT Press, London, 1992.

[6] Y. Trivedi, "Wireless power transfer: "Look ma, no hands, no wires!""", *IEEE Communications Magazine*, Vol. 54, Issue 7, July 2016, pp. 8-13. Doi: 10.1109/MCOM.2016.7514157

# Distributed Optical Fiber Sensor and Its Various Applications

Madhushree Sharma<sup>1</sup>, Shakuntala Laskar<sup>2</sup>

<sup>1</sup>Department of Electronics and Communication Engineering, Girijananda Chowdhury Institute of Management, Airport Road, Azara, Guwahati, Assam  
*ms.madhushree.sharma@gmail.com\**

<sup>2</sup>Department of Electrical and Electronics Engineering, School of Technology, Assam Don Bosco University, Airport Road, Azara, Guwahati -781017, Assam, INDIA.  
*shakuntala.lashkar@dbuniversity.ac.in*

**Abstract:** *The process of sensing can also be done with the help of optical fiber. This method of sensing is becoming very popular. The optical communication, which is the main communication technology, in this case, takes light as the carrier and optical fiber as the communication medium. Distributed Optical Fiber Sensors (DOFS) can be used for continuous measurement at the same time to obtain the spatial distribution of the measured state and time-varying information. This paper describes the background of DOFS technology. Various applications of DOFS are also listed.*

**Keywords:** Distributed Optical Fiber Sensor (DOFS), Fiber Bragg Grating (FBG), Structural Health Monitoring (SHM)

## 1. Introduction

We can use the process of multiplexing, where there are multiple numbers of inputs and a single output, to increase the function ability of the optical fiber sensor [1]. A common optoelectronic terminal can be used, thereby reducing the cost to a very large amount. In a distributed sensor, the sensor consists of a single length of the fiber cable and the optoelectronic terminal can monitor the variation of a physical parameter such as temperature, pressure, water level etc. In a Distributed Optical Fiber Sensor (DOFS), this sensing should be a continuous process. Distributed sensing replaces the complex integration of thousands of sensor with one optical fiber system. The inherent distributed sensing nature of fiber-optic sensors can be used to create unique forms of sensors for which, in general, there may be no counterpart based on conventional sensor technologies. The basic advantage of optical fiber is that it is cheap, light, pliable and are immune to Electro-Magnetic Interference (EMI). This is an inherent sensor medium with low cost, inertness and flexibility. The fiber is a flexible, insulating, dielectric medium, which can be readily installed in an industrial plant without significant disturbances of the measurement environment [2,12].

## 2. Working Principle and Measuring Techniques

Temperature, pressure and tensile strength etc. change the characteristics of light transmission in a

fiber. A damping or attenuation is caused by these external physical parameters and their exact location can be found out by the method of scattering. Thus, the optical fiber can be employed as a sensor. The quartz that consists of  $\text{SiO}_2$  is the basic component of optical fiber. Any variation in the external parameter will induce some oscillations in the structure. When light falls onto these thermally excited molecular oscillations, an interaction occurs between the light particles (photons) and the electrons of the molecule, thereby causing a phenomenon known as the Raman Scattering. This scattered light from the optical fiber consists of three different components as mentioned below [3]:

- (i) **Rayleigh Scattering Component:** It is the dominant component that has the frequency, same as the frequency of the laser source being used in the system.
- (ii) **Stokes Line Component:** This component consists of lower frequency optical signals than the Rayleigh scattered component.
- (iii) **Anti-Stokes Line Component:** This component consists of higher frequency optical signals than the Rayleigh scattered component.

## 3. Measurement Methods

For the measurement of different scattered components in a DOFS, we can basically use three methods:

- (i) **Optical Time Domain Reflectometry (OTDR):** This was developed more than 20 years ago. Here, a narrow laser pulse generated by a semiconductor or solid-state laser is sent into the fiber and the back-scattered light is analyzed. From the time duration that it takes the back-scattered light to return to the detection unit, it is possible to locate the origin of the external physical parameter such as increase or decrease in temperature, pressure, tensile force etc.
- (ii) **Optical Frequency Domain Reflectometry (OFDR):** Here, the back-scattered light is measured as a function of frequency and Fourier transformation is used.
- (iii) **Code Correlation Optical Time Domain Reflectometry (CC-OTDR):** Here, binary Coley Code is used and the optical energy is spread over a code rather than packed into a single pulse.

#### 4. Basic Structure of a DOFS System

DOFS basically, consists of a controller, laser source, and pulse generator for OTDR or CC-OTDR, modulator, high frequency (HF) mixer for OFDR, optical module, receiver, microprocessor unit and a quartz glass fiber as a sensor medium.

#### 5. Various Applications of DOFS

There are numerous applications of Distributed Optical Fiber Sensor (DOFS) network including monitoring of embankment dams, pipeline leakage detection, habitat monitoring and structural health monitoring etc. Various applications are listed below:

- (a) **Monitoring Embankment Dams:** The usual method of monitoring of embankment dams uses the pneumatic piezometers that measure the gas pressure and the readings are taken weekly in a manual manner. The sunlight will cause severe damage to the piezoelectric component. These problems can be solved by the fiber optic sensor. A fiber optic sensor system based on fiber bending loss and optical time domain reflectometry (OTDR) can be used for monitoring of embankment dams [4]. This system uses an OTDR module that sends pulses to the distributed sensors placed in the embankment dams. The attenuation of the reflected pulses due to the external pressure is measured that will give the level of water penetration in the embankment dams.
- (b) **Pipe Line Leakage and Intrusion:** It is always a problem to monitor or check the underground pipe line leakage, tampering and overload of any form. A distributed optical fiber sensor (DOFS) was proposed to monitor the pipe line leakage and intrusion that is based on Code Correlation OTDR (CC-OTDR) that uses the Golay Codes. The transmitted and the reflected optical power are correlated and the loss is obtained. This loss is sensitive to the soakage of the hydrocarbon fuels and the intrusion such as tampering, overload, impacting etc. The CC-OTDR improves the range of frequency that can be analyzed and also improves the signal to noise ratio compared to the conventional OTDR [5].
- (c) **Virtual Monitoring of Rotor Temperature:** Rotor temperature of a turbine has a direct relationship with the turbine's safe running and safety. A Distributed Optical Temperature Sensor (DOFS) is used to obtain the overall temperature of the rotor rather than the temperature of a particular place by using a single sensor. This is a low cost, more convenient, fast and high precision method compared to the single sensor method. The Laboratory Virtual Instrument Engineering Workbench (LabView) software can be used for virtual monitoring of the rotor temperature [6].
- (d) **Power System Temperature Monitoring:** The Distributed optical fiber Temperature Sensor (DTS) uses the Raman scattering effect. This technique is a continuous method to monitor the temperature that can operate safely in the dangerous power system environment. When the temperature of the power station exceeds the set value, an alarm signal will be sending out. Two engineering project work of China are monitored by this method where they use the temperature set point at 78°, after which the alarm signal will be sent out [7].
- (e) **Measurement of Structural Strain:** The Brillouin optical time-domain reflectometer method can be used to monitor structural strain. This method can measure strain at points along continuous lengths of the optical fiber of up to 10 km and more. Whenever there is a fault in a civil structure, this method can provide an effective warning measure [8]. This method uses a nonwoven cloth that can detect soil movements of a few millimetres in soil structure.
- (f) **Smart Sensor for SHM:** A smart transducer interface module is developed that is made up of 2 optical fiber PIN receiver, a differential amplifier and a digital signal processor. The

DSP unit consists of an in build analog to digital converter (ADC). Here [9], a smart transducer interface module (STIM) for Fiber Bragg Grating (FBG) sensor to realize Optical Fiber Sensor (OFS) is developed. Typically, FBGs are used as spectral transduction elements due to the absolute nature of spectral encoding and immunity to optical power fluctuation. FBGs have several characteristics such as small size, small weight, immune to the electromagnetic effect, versatility to detect various physical measurands. These characteristics make FBGs very much reliable for structural health monitoring (SHM). Acoustic emission, actively generated acoustic-ultrasonic signal, dynamic strain (e.g. vibration), static strain (load monitoring), and corrosion, etc. come under SHM.

- (g) **DTS with Optical Switch:** Distributed optical fiber temperature sensor (DTS) is a real-time, online, continuous optical fiber temperature measurement system. It has become a new detection method and technology for the field of public safety and industrial process monitoring. In DTS, the length of the sensing optical fiber is determined by the power of laser pulse, loss coefficient and Signal to Noise Ratio (SNR) of the system. By the introduction of optical switch, we can extend the sensing length of the system [10]. The high-frequency anti-Stokes Raman scattering signal in optical fiber is modulated by spatially distributed temperature field while the Stokes Raman scattering signal is not. Temperature value at any point along the optical fiber can be calculated by using Stokes Raman scattering signal to demodulate anti-Stokes Raman scattering signal. DTS is based on this concept. The temperature is calculated out by the ratio of anti-Stokes Raman and Stokes Raman signals.
- (h) **DTS for Hydrologic System:** Hydrologic processes are strongly influenced by interacting processes that span spatial scales from centimetre to kilometres, presenting profound challenges for description, modelling and observation. By placing many sensor nodes spaced along the distance, it would be possible to observe hydrologic processes.
- (i) **Audible Frequency Sensor:** After the discovery of Cole and Bruno in the year 1977, that sound can be detected by the optical fiber; many types of research are going on in this field. A Distributed Optical Fiber Sensor (DOFS) has been demonstrated that uses in-phase Optical Time Domain Reflectometer (OTDR) technique to detect acoustically generated perturbation along the sensing fiber.

The result shows that this technique can measure both the frequency and the amplitude of multiple perturbations. We can also use a Chebyshev window in the signal processing procedure to improve the Signal to Noise Ratio (SNR) value.

- (j) **Vibration Sensor:** An Optical Time Domain Reflectometer (OTDR) is developed to achieve high-frequency response and wide spatial resolution. Pencil-break event is tested as a vibration source. OFDR can also be used for vibration sensing. A distributed vibration sensing system based on all polarization-maintaining configurations of the phase sensitive OTDR can be presented.

## 6. Conclusion

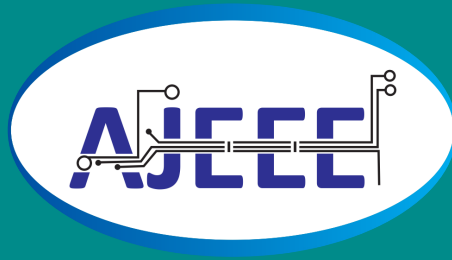
Distributed Optical Fiber Sensors (DOFS) is a new technology where the transmission medium itself acts as a sensor. This technique can be used to detect various faults in the civil structures, leakage in the buried pipelines, the pressure exerted in a device, frequency, vibration etc. It is gaining very wide use due to its low cost and immunity towards electromagnetic interference. This paper discusses the characteristics of DOFS and its various applications.

## References

- [1] J. P. Dakin, "Multiplexed and Distributed Optical Fiber Sensors", *Proc. of International Symposium on Advanced materials for lightweight structures (ESA SP-336, October 1992)*, ESTEC, Noordwijk, The Netherlands, 25-27 March, 1992, pp. 385-392. Retrieved from <https://eprints.soton.ac.uk/393679/1/711.pdf>
- [2] A. J. Rogers, "Distributed optical-fibre sensors for the measurement of pressure, strain and temperature", *Journal of the Institution of Electronic and Radio Engineers*, Vol. 58, Issue 5 (Supplement), July-August 1988, pp. S113-S122. Doi: 10.1049/jiere.1988.0048
- [3] G. J. Cowle, J. P. Dakin, P. Morkel, T. P. Newson, C. N. Pannell, D. N. Payne and J. E. Townsend, "Optical fiber sources, amplifiers, and special fibers for application in multiplexed and distributed sensor systems", in *Distributed and Multiplexed Fiber Optic Sensors*, A. D. Kersey and J. P. Dakin (eds.), SPIE Conference Volume 1586, Boston, MA,

- United States, 1-7 September 1991, pp. 130-145. Doi: <https://doi.org/10.1117/12.56513>
- [4] L. A. Ribeiro, J. B. Rosolem, D. C. Dini, C. Floridia, C. A. Hortencio, E. F. da Costa, E. W. Bezerra, R. B. de Oliveira, M. D. Loichate and A. S. Durelli, "Fiber optic bending loss sensor for application on monitoring of embankment dams", *Proc. of 2011 SBMO/IEEE MTT-S International Microwave and Optoelectronics Conference (IMOC 2011)*, Natal, 29 Oct.-1 Nov. 2011, pp. 637-641. Doi: 10.1109/IMOC.2011.6169273
- [5] Y. Wang, Z. Li and Z. Jiang, "An improved distributed optical fiber sensor (DOFS) for monitoring long-distance buried oil pipeline leakage and intrusion", *Proc. of 2009 4th IEEE Conference on Industrial Electronics and Applications*, Xi'an, China, 25-27 May 2009, pp. 318-320. Doi: 10.1109/ICIEA.2009.5138220
- [6] L. Wang, X. Yang and B. Sheng, "Distributed Optical Fiber Sensor for Virtual Monitoring of Turbine Rotor's Temperature", *Proc. of 2009 International Conference on Measuring Technology and Mechatronics Automation*, Zhangjiajie, Hunan, 21-22 April 2009, pp. 16-19. Doi: 10.1109/ICMTMA.2009.215
- [7] C. Hu, J. Wang, Z. Zhang, S. Jin and Y. Jin, "Application Research of Distributed Optical Fiber Temperature Sensor in Power System", in *Optical Sensors and Biophotonics*, J. Popp, D. Matthews, J. Tian, and C. Yang (eds.), Vol. 8311 of Proceedings of SPIE (Optical Society of America, 2011): 2011 Asia Communications and Photonics Conference and Exhibition, Shanghai China, 13-16 November 2011, Paper 83112E.
- [8] M. Kihara and H. Ohno, "Distributed Optical Fiber Sensor using Brillouin Scattering", *Proc. of 2003 Conference on Lasers and Electro-Optics/Quantum Electronics and Laser Science Conference (CLEO'03)*, Baltimore, United States, 1-6 June 2003, Paper CFC3.
- [9] G. Wild and S. Hinckley, "Distributed optical fibre smart sensors for Structural Health Monitoring: A Smart Transducer Interface Module", *Proc. of 2009 International Conference on Intelligent Sensors, Sensor Networks and Information Processing (ISSNIP)*, Melbourne, VIC, 7-10 Dec. 2009, pp. 373-378. Doi: 10.1109/ISSNIP.2009.5416754
- [10] J. Wang, Y. Jin, Z. Zhang, C. Shen and Y. Qiu, "Research of Distributed Optical Fiber Temperature Sensor (DTS) System with Optical Switch", *Proc. of 2010 Symposium on Photonics and Optoelectronics*, Chengdu, China, 19-21 June 2010, pp. 1-4. Doi: 10.1109/SOPO.2010.5504447
- [11] J. S. Selker, L. Thévenaz, H. Huwald, A. Mallet, W. Luxemburg, N. van de Giesen, M. Stejskal, J. Zeman, M. Westhoff and M. B. Parlange, "Distributed fiber-optic temperature sensing for hydrologic systems", *Water Resources Research*, Vol. 42, Issue 12, Dec. 2006, W12202. Doi: <https://doi.org/10.1029/2006WR005326>
- [12] A. Barrias, J. R. Casas and S. Villalba, "A review of distributed optical fiber sensors for civil engineering applications", *Sensors*, Vol. 16, Issue 5, Article 748, May 2016. Doi: <https://doi.org/10.3390/s16050748>





## **ADBU Journal of Electrical and Electronics Engineering**

ISSN: 2582-0257

[www.tinyurl.com/ajejee-adbu](http://www.tinyurl.com/ajejee-adbu)

**ASSAM DON BOSCO UNIVERSITY**

Azara Campus, Airport Road, Guwahati - 781017

+91-9435545754, 0361-2139291/92

[www.dbuniversity.ac.in](http://www.dbuniversity.ac.in)